Ecological Indicators 130 (2021) 108092

Contents lists available at ScienceDirect

Ecological Indicators

journal homepage: www.elsevier.com/locate/ecolind

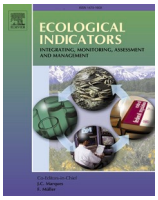

Coupling linear spectral unmixing and RUSLE2 to model soil erosion in the Boubo coastal watershed, Côte d'Ivoire

Lenikpoho Karim Coulibaly [a], Qingfeng Guan [a,b,*], Tchimou Vincent Assoma [c], Xin Fan [d], Naga Coulibaly [e]

[a] School of Geography and Information Engineering, China University of Geosciences, Wuhan, Hubei Province, China
[b] National Engineering Research Center of GIS, China University of Geosciences, Wuhan, Hubei Province, China
[c] University Center for Research and Application in Remote Sensing (CURAT), University of Félix Houphouet Boigny, Abidjan, Côte d'Ivoire
[d] School of Public Administration, China University of Geosciences, Wuhan, Hubei Province, China
[e] Laboratory of Geoscience and Environment, UFR of Science and Environmental Management, Nangui Abrogoua University, Abidjan, Côte d'Ivoire

ARTICLE INFO

Keywords:
Soil erosion
RUSLE2
Linear spectral unmixing
Climate change
GIS
Remote sensing

ABSTRACT

Water erosion accelerates soil degradation through land use, land cover, and climate change. Accurate modeling of soil erosion is critical for assessment of environmental variables such as nutrient loss, reduction of soil fertility, and water quality degradation. Modeling of soil erosion can provide insights to conservation planners for formulating policies to prevent land degradation. However, when used for soil erosion modeling in Geographical Information Systems (GIS), application of the Revised Universal Soil Loss Eq. (2) (RUSLE2) is realized based on the assumption that the pixels of land use data are pure and that mixed land use units within pixels can be ignored, and this opposes the accurate estimation of regional soil erosion. The methodology developed in this study includes combination of the GIS-based RUSLE2 with linear spectral unmixing (LSU) to analyze the change in vegetation cover within a pixel and to improve the spatial representation of the soil erodibility factor using climate data derived from the Boubo coastal watershed. The findings reveal that the estimated monthly erosivity density in the Boubo coastal watershed for different months varies between 0.05 and 20.86 MJ mm $ha^{-1}h^{-1}$ $year^{-1}$ in 1990 and 0.8 to 21.21 MJ mm $ha^{-1}h^{-1}$ $year^{-1}$ in 2019. The geographical soil erodibility K-factor varied between 0.008 and 0.022 t.ha.h.ha^{-1}.MJ^{-1}.mm^{-1}. The temporal soil erodibility K_J factor was highest in May 1990 (0.194) and June 2019 (0.2). Slopes varied between 0% and 56%, with LS values exceeding 16. The deforestation rate in the Boubo coastal watershed was 65.49% from 1992 to 2019. The mean soil loss rate in June was 0.048 t/ha/month in 1990 and was 0.073 t/ha/month in 2019. Sediment yield increased from 1.09 t/ha/yr in 1990 to 2.54 t/ha/yr in 2019. Based on the RUSLE2 empirical equation, it was inferred that the estimated sediment transport capacity increased during the baseline period. Further studies should be conducted to evaluate ecosystem management based on ecosystem services and sediment deposition in this area.

1. Introduction

Soil degradation through accelerated water erosion is a grave concern, particularly in developing countries in the tropics (Bai et al., 2008; Lal, 2001). Soil loss has been recognized as a potential ecological, environmental, social, and economic problem because of its effects (Garcia-Ruiz et al., 2016; Wuepper et al., 2019; Xin, 2020; Jianxiang et al., 2019). Thus, approaches for soil erosion prevention have garnered considerable attention worldwide (Xin and Lin, 2020). Globally, more than 1642 million hectares of land are eroded (Li and Fang, 2016). In Africa, the intensity of water erosion has been described as very high to extreme for approximately 45 percent of the continent in the south of the Sahara (SSA) area, and has been deemed moderate for approximately 30 percent and slight for approximately 25 percent (FAO, 2015; Oldeman, 1992). Modeling of soil erosion can provide guidance to decision-makers and managers to formulate adequate land management measures in the study area.

Several models have been established for soil loss assessment, such as the Universal Soil Loss Equation (USLE), Revised Universal Soil Loss Equation (RUSLE), RUSLE2, LImburg Soil Erosion Model (LISEM), Water

* Corresponding author at: School of Geography and Information Engineering, China University of Geosciences, Wuhan, Hubei Province, China.
E-mail address: guanqf@cug.edu.cn (Q. Guan).

https://doi.org/10.1016/j.ecolind.2021.108092
Received 28 April 2021; Received in revised form 4 August 2021; Accepted 7 August 2021

Erosion Prediction Project (WEPP), Pan European Soil Erosion Risk Assessment (PESERA), Hillslope Erosion Model (HEM), and EROSION-3D (Dutta, 2016; Karydas et al., 2012; Patil, 2018). The number of input data and their complexity, processes considered, and type differ with respect to the model considered. Machine learning methods have recently been used to map soil erosion (Cheng et al., 2018). However, the application of this method in the estimation of soil erosion in several areas has remained challenging because of limitations in data availability (Xu et al., 2019). Among various erosion models, USLE and its family models are widely and most commonly used in the modeling of soil erosion (Kinnell, 2019). These family models can be used at a national scale (Benaud et al., 2020; Grazhdani and Shumka, 2007; Schmidt et al., 2019; Teng et al., 2019), in larger watersheds with diverse land use (Latocha et al., 2016; Pirnazar et al., 2018), at a watershed scale (Panagos et al., 2012; Phinzi and Ngetar, 2019), on a small scale (Meusburger et al., 2010b; Mondal et al., 2016), and at plot scales (Lewis, 2013; Roose, 1975). However, previous studies have reported the use of USLE and its family models (Abdulkareem et al., 2019; Kijowska-Strugała et al., 2018; Roose, 1977) but did not consider temperature variations.

RUSLE2 is a hybrid empirical/process-based model that is used by combining the best empirical and process-based erosion prediction methods prescribed by the United States Department of Agriculture (USDA) (USDA-ARS, 2008; USDA-ARS, 2013; USDA, 2001). Issues encountered in the previous models can be solved by integrating data on temperature into the soil erodibility equation, and integration with GIS enables easy execution of erosion studies based on mixed pixels of land use. It is a well-validated technology for predicting erosion and is suitable for predicting erosion in most cultivated land types in West Africa (Roose, 1996). Furthermore, RUSLE2 was developed using modern theories on soil particle detachment, transport, and deposition by the raindrop effect and surface runoff.

Estimation of fractional vegetation cover is a key procedure in soil erosion estimation and ecological restoration studies. Assessment of the change in soil erosion and depiction as vegetation cover changes are essential for understanding the restoration efficiency and ecosystem functions of soil erosion control and for evaluating ecosystem services (Fu et al., 2011). Various methods have been widely used to estimate the fractional green cover (FGC) (García-Haro et al., 2019; Song et al., 2017; Vrieling, 2006; Xu et al., 2019; Yang, 2014; Zhang et al., 2019; Zhao et al., 2020). The linear spectral unmixing method (LSU) (Asner and Heidebrecht, 2002), mixture tuned matched filtering method (MTMF) (Meusburger et al., 2010a), and machine learning methods (Baret et al., 2013) are also used to estimate FGC. In soil erosion studies, one condition necessary to accurately estimate soil loss based on RUSLE2 is the precise determination of the cover management factor (C factor) because the surface cover exerts a more pronounced effect on soil loss than any other factor (Foster et al., 1999; Vijith et al., 2017). Researchers have suggested many methods that can be used for estimating the C factor at different scales (Qiang and Wenwu, 2014; Tanyaş et al., 2015). The main methods at the regional and watershed scales are as follows. Firstly, the original method is used to estimate the C factor based on data derived from field work and experiments (Renard et al., 1997; Spaeth et al., 2003); however, one limitation of this approach is that it is based on tests conducted using collected samples. This method requires the inclusion of a standard community and long-term monitoring, and these cannot be easily implemented (Tanyaş et al., 2015). Secondly, researchers have considered normalized difference vegetation (NDVI) to map the C factor using regression analysis (Almagro et al., 2019; Ayalew et al., 2020; Pham et al., 2018; Vatandaşlar and Yavuz, 2017). Karydas et al. (2009) used a fuzzy sigmoid transformation of NDVI values to map the C factor. Yang (2014) proposed a monthly NDVI-based C factor. However, this method requires the inclusion of additional monthly remote sensing data that cannot be easily obtained in the areas where data are missing, and where the C factor and vegetation indices show poor correlation (De Jong, 1994; Montandon and Small, 2008; Panagos et al., 2015). Thirdly, researchers assign C factor values according to the land use type (Farhan and Nawaiseh, 2015; Kidane et al., 2019; Olorunfemi et al., 2020). However, this method cannot be used to accurately represent the change in vegetation across large areas (Pan and Wen, 2013; Tanyaş et al., 2015; Wang et al., 2002). Fourthly, the C factor data are extracted using the inverse method based on application of the RUSLE equation after field measurement of other variables. However, data cannot be easily obtained in most cases (Tanyaş et al., 2015). Fifthly, Mapping of C factor values can be improved by adopting geostatistical methods based on the use of remote sensing images (Gertner et al., 2002; Wang et al., 2002). Although spatial statistical analysis has been performed comprehensively, the workload required is markedly considerable, and the application is difficult. Sixthly, studies have reported the combination of existing methods of C factor estimation. The combination of remote sensing data at a high spatial resolution with information from existing literature reviews in the study area and field data can improve the C factor mapping (Panagos et al., 2015; Tanyaş et al., 2015). However, this approach determined the C factor via the application of NDVI index ignoring the mixed pixels of land use. The resulting spatial variation in the C factor is inaccurate. Additionally, mapping the C factor of the study area is based on acquisition of considerable data and conduction of extensive previous work. Seventhly, recent studies used a machine learning approach to predict C-factor maps (Tsai et al., 2021). Finally, the C factor values also have been estimated by performing linear spectral mixture analysis (De Asis and Omasa, 2007; Lu et al., 2004). Studies have demonstrated that the linear spectral mixture model is a more accurate method than the NDVI-based linear mixture model (Yang et al., 2012; Zhao et al., 2020). De Asis and Omasa (2007) proposed a new method for calculating the C factor using linear subpixel unmixing (LSU). De Asis et al. (2008) noted that the LSU technique, when applied to Landsat data, offered a more accurate assessment of land conditions related to soil erosion in tropical watersheds, such as the Boubo coastal watershed. Although the method is theoretically imperfect because the impact of distribution between different land cover types is not considered (Myneni et al., 1995; Roberts et al., 1993), the errors resulting from linear assumptions are relatively minor (Kerdiles and Grondona, 1995). LSU has also been proven to be a good tool for estimating endmember fractions (Adams and Smith, 1986; Elmore et al., 2000; Small, 2003) and is widely used because of its simplicity, interpretability, and effectiveness (Xiao and Moody, 2005). In the present study, owing to the lack of availability of data, the LSU was deemed suitable and proved advantageous for decomposing mixed pixels. The main advantage of automatic LSU classification is the conduction of rapid data processing. It is a time-saving, inexpensive, and relatively simple method that can be used over large areas (Žížala et al., 2018). The potential erosion areas are estimated at the mixed pixel level. Comparison studies have indicated that LSU results are better than those obtained via consideration of vegetation indices (Jimenez-Munoz et al., 2009).

Another condition necessary to precisely estimate soil loss is the accurate estimation of an essential factor for the RUSLE2 model, that is, the spatiotemporal variation in the soil erodibility K factor. This factor reflects the regional soil erodibility (USDA-ARS, 2013). Several authors have used the classical soil erodibility factor equation to determine the K factor (Teng et al., 2019; Xin, 2020). However, the classical K factor equation, rather than the nomograph, should be used with caution in these studies because the classical equation would lead to incorrect predictions in more than 50% of cases (Auerswald et al., 2014). The use of Wischmeier's monograph to determine the geographical K factor is adapted to most regions of West African land (Roose, 1975). Villemure used this method in West Africa (Villemure, 2006) and concluded that ferrallitic soil was markedly resistant to erosion (K ranged from 0.01 to 0.2). Furthermore, several studies have been conducted by considering soil erodibility (K factor) as a parameter that is constant for a year for a given soil and have shown that stable soil properties can be used to assess soil erodibility (Karydas et al., 2013; Wang et al., 2016). However,

other studies have found that soil erodibility varies over the year for a given soil due to location, climate change, and human activity (Kinnell, 2010; Ostad-Ali-Askari et al., 2019; USDA-ARS, 2013). Therefore, soil erodibility should be considered as a variable term that changes over time and space rather than one that remains constant (Kinnell, 2019; Ostad-Ali-Askari et al., 2020; Wang et al., 2013). USDA-ARS (2013) noted that the temporal soil erodibility factor could be determined by using temperature data and proposed a method to estimate the temporal K factor using information on temperature, which highlighted a new strategy for optimization of the RUSLE2 model.

Soil erosion is most often accompanied by sediment transport. Water flow transports sediment downslope (Ostad-Ali-Askari et al., 2016). Sediment yield and runoff are two critical soil erosion parameters (Zhu et al., 2018). Changes in land cover affect runoff and sediment yield by changing the canopy structure and ground cover (Borrelli et al., 2015; Liu et al., 2018; Maeda et al., 2013; Wan et al., 2012). Sediment yield is a critical factor considered for detecting non-point source (NPS) pollution. Estimation of runoff and sediment yield is vital because the sediment produced may carry pollutants (Jebari et al., 2012; Lanckriet et al., 2016; Ostad-Ali-Askari and Shayannejad, 2021), and pollutants may affect agricultural productivity (Golian et al., 2020; Gu et al., 2018; Lal, 2001; Lal, 2014; Zhu et al., 2018) and degrade water quality (Lal, 2015). Additionally, when runoff begins, the amount and the size of the transported material are determined by estimating the transport capacity (Tc) of water from runoff. If the transport capacity is insufficient to transport the available eroded soil material, the sediment that exceeds the capacity of transport is deposited (Jain and Das, 2009; Jain et al., 2009).

The present study aimed to combine GIS-based RUSLE2 and LSU and used LSU to determine the C factor and to improve the results of the RUSLE2 model. Temporal temperature data were also used to perform adjustments for the soil erodibility to improve the accuracy of the RUSLE2 model.

The proposed framework was applied to the Boubo coastal watershed to estimate the soil erosion dynamics. The Boubo coastal watershed has been selected from the main 11 watersheds in Côte d'Ivoire because it plays an important role in the physical, biological, and hydrological exchange between lagoons and the sea. Unfortunately, its rivers are not considered in national monitoring planning (Sébastien et al., 2013). Moreover, this important large coastal watershed presents only two hydrometric stations and two rain gauge stations, which poses challenges in rainfall erosivity estimation and in the conduction of climate change studies. Boubo is an agricultural area in which fertilizers and pesticides are widely used. The changes in land use over the last 29 years in the Boubo coastal watershed have resulted in significant sediment deposits in the lagoon. Fisheries resources, such as fresh fish, are highly threatened. Additionally, despite the importance of this coastal watershed, markedly few studies related to erosion and sediment yield have been conducted in this area (Kouadio, 2011; Milliman and Farnsworth, 2011; Vanmaercke et al., 2014). Most studies in Côte d'Ivoire focus on the Bandama, San Pedro, Comoe, Sassandra, and Agneby watersheds. This study demonstrates advantages and is based on principles of government and conservation planning.

Provision of guidelines for the reduction of waterborne erosion based on information on the geographic location, land use/cover, climate, and funding conditions is challenging because of the lack of availability of studies and data in this area. This study focuses on modeling and mapping of soil erosion potential and estimation of the sediment yield risk and delivery ratio in the Boubo coastal watershed. We reviewed previous studies conducted worldwide, examined changes in vegetation cover, and used available data to generate erosion risk maps. The results of this study can provide useful information and may help managers and planners in the formulation of policies to protect the ecological environment of the study region.

2. Study area and datasets

2.1. Study area

Boubo is a north–south watershed that is over 130 km in length. It covers an area of almost 5048.27 km^2 (Fig. 1). Slopes varying from 0% to 5 % occupy more than 52% of the Boubo watershed, indicating that the study area generally exhibits a flat surface (Table 1). Flat slopes are ideal for the application of RUSLE2 (Foster et al., 1999). The Boubo watershed intersects the Atlantic Ocean via the Makey Lagoon in Côte d'Ivoire. The climate is a sub-equatorial (two rainfall seasons) type with an annual rainfall exceeding 1500 mm/year. Boubo presents with two rainy and two dry seasons. The Great Rainy Season lasts from mid-March to mid-July; the short rainy season covers the months of September and October. The great dry season extends from November to mid-March, and the short dry season extends from mid-July to the end of August. The average temperature of the basin ranges between 25 °C and 27 °C. The main activity in Boubo is agriculture, which represents almost 80% of the total human activity in the region (Kouadio, 2011). The Boubo watershed is part of the southern Ivorian forest (Avenard et al., 1971). The swamp forests, dense evergreen forests, Diospyros spp. (Ebénacées), and Mapania spp. (Cyperaceae) thrive on soils with a high water retention capacity, and are recognized as the four types of vegetation in Boubo (Avenard et al., 1971).

2.2. Datasets and data processing

The illustration of the boundary of the Boubo watershed was produced using a digital elevation model (DEM). Satellite images were acquired during the dry season. During this period, the sky was not covered by clouds; therefore, most areas exhibited almost 100% exposed soil. By applying primary pre-processing operations and by using LSU, land cover fractions for the years 1990 and 2019 were obtained for the study region. The other data used in this study are listed in Table 2.

3. Methods

3.1. Application of the RUSLE2 model

The approach used herein was based on the execution of a diachronic study of water erosion. The raster maps developed for the r_i, k_i, l_i, S, c, and p factors of the RUSLE2 model were combined to estimate, to evaluate, and to generate maps of soil loss and severity. Fig. 2 shows the flow chart of RUSLE2, which can be used to establish precipitation, soil type, elevation, and land cover data layers and the corresponding derivations from these layers (USDA-ARS, 2008). This model is used to compute the long-term average soil loss, using the equation expression as follows:

$$A = \frac{\left(\sum_{i=1}^{365N} r_i k_i l_i \mathrm{S} c_i p_i\right)}{N} \quad (1)$$

where A represents the annual soil loss; r_i denotes the daily erosivity factor ($MJ.mm.ha^{-1}.h^{-1}.year^{-1}$), k_i represents the daily soil erodibility factor ($t.ha.h.ha^{-1}.MJ^{-1}.mm^{-1}$), l_i represents daily slope length factor (dimensionless), S represents daily slope steepness factor (dimensionless), c_i represents daily cover management factor (the C factor, dimensionless), which can be determined by adopting the LSU method; p_i denotes the daily support practice factor (dimensionless); all long-term averages are indicated for the ith day, and N represents the total number of years in the calculation. The lowercase symbols represent daily values. In case of USLE and RUSLE1, uppercase symbols are used to denote annual values.

3.1.1. Estimation of the C factor using LSU

The cover management factor (C-factor) was determined using the

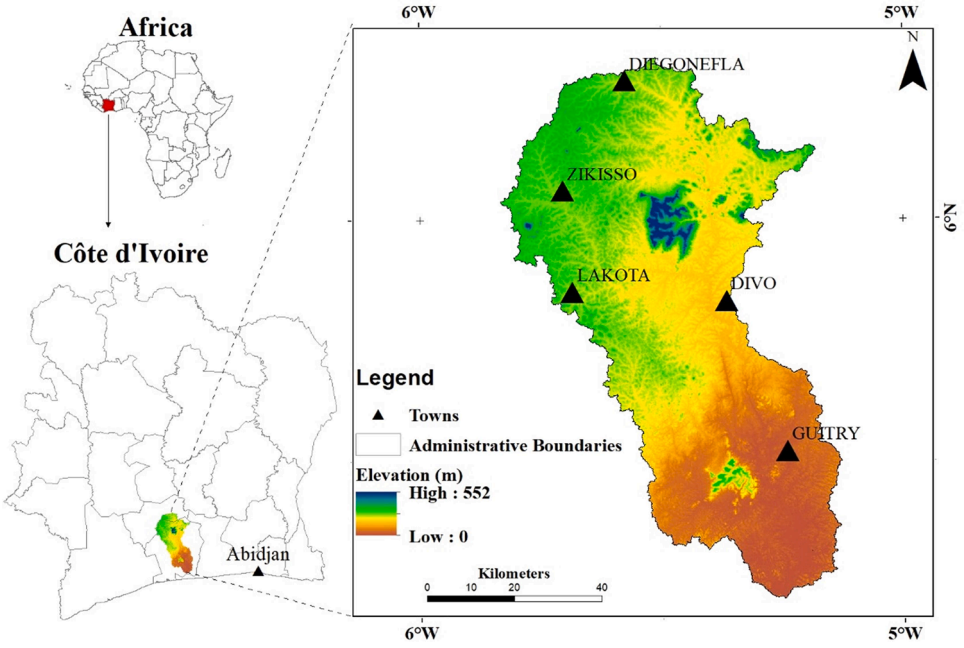

Fig. 1. Location map of the Boubo coastal watershed.

Table 1
Classification of slopes in the Boubo watershed.

No.	Slope category	Slope (%)	Area	
			Km^2	%
1	**Nearly level**	0–5	2668,39	52,86
2	**Gentle slope**	5–10	1757,30	34,81
3	**Moderate slope**	10–20	565,63	11,20
4	**Steep slope**	20–56	56,94	1,13

LSU model in the present study. We used the ENVI 5.1 software to classify ground fractions through LSU. We obtained spectral unmixing results by combining automatic minimum noise fraction (MNF) and supervised pixel purity index (PPI) endmember selections by processing Landsat 5 ETM + and Landsat 8 Operational Land Imager (OLI) images. The MNF-PPI demonstrates the advantage of being used for separation of pure pixels from those that are more mixed, thereby minimizing the number of pixels that must be examined and simplifying endmember separation and identification. Previous research has shown that application of MNF can improve the quality of fraction images through decorrelation. The most spectrally pure pixels in the images were obtained using PPI. The C factor is defined on a pixel-by-pixel basis using this equation (De Asis and Omasa, 2007) expressed as follows:

$$C = \frac{F_{bs}}{1 + F_{veg} + F_{NPM}} \quad (2)$$

where F_{bs} denotes the fraction of bare soil: the bare soil endmember information was collected from Landsat images; F_{veg} denotes different forest tree species in the Boubo watershed; and F_{NPM} represents non-photosynthetic material. The data on endmembers for the NPM were derived from open spaces, abandoned cultivated fields, branches, rocks, dried leaves, or gravel.

The unmixing was constrained to ensure that every endmember's fraction ranged between 0 and 1, and for each pixel, the sum of fractions equaled 1 (Adams and Smith, 1986; Smith et al., 1990). All input layers were enhanced into the raster layer for application in the RUSLE2 model. Each of the RUSLE2 factors was calculated separately and was adapted to the specific environmental conditions of the Boubo watershed. We used the classified Landsat images in Google Earth Engine (GEE) to validate the accuracy of the LSU. The LSU validation can be performed during fieldwork by collecting samples for validation (De Asis et al., 2008) or by using remote sensing data (Huang et al., 2020; Papaiordanidis et al., 2020). Based on the consideration of remote sensing and GIS development, GEE provides a good alternative for validating this type of study over a large area. GEE has been proven to be reliable, provides a good basis for analysis, and is considered time-saving while providing good results (Shelestov et al., 2017; Sun et al., 2019; Tadele et al., 2017; Wahap and Shafri, 2020). The ENVI 5.1 software provides automatic RMSE of the classification. The RMSE represents a better model performance than MAE (Chai and Draxler, 2014). In LSU studies related to erosion, the RMSE has often been used to evaluate land use classification (Pan and Wen, 2013). A small RMSE indicates that the selected endmembers are sufficient and valid (Pan and

Table 2
List of datasets used in this study.

Category	Dataset (format)	Source	Spatial resolution	Temporal period	Variables
DEM	Alos palsar L-band (raster)	Alaska Satellite Facility (https://www.asf.alaska.edu)	12.5 m	July 2007	Elevation
Climate	Temperature Precipitation	NASA POWER (https://power.larc.nasa.gov)	Grid, 0.25*0.25°	Years 1990–2019	Daily precipitation and temperature
Soil	Pedology map of the Boubo watershed	FAO database (http://www.fao.org)	1:5 000 000		Sand, silt, and clay fractions; organic matter %
Land cover	Landsat images	USGS Global Visualization Viewer (https://glovis.usgs.gov)	30 m	Years 1990–2019	Land cover fractions

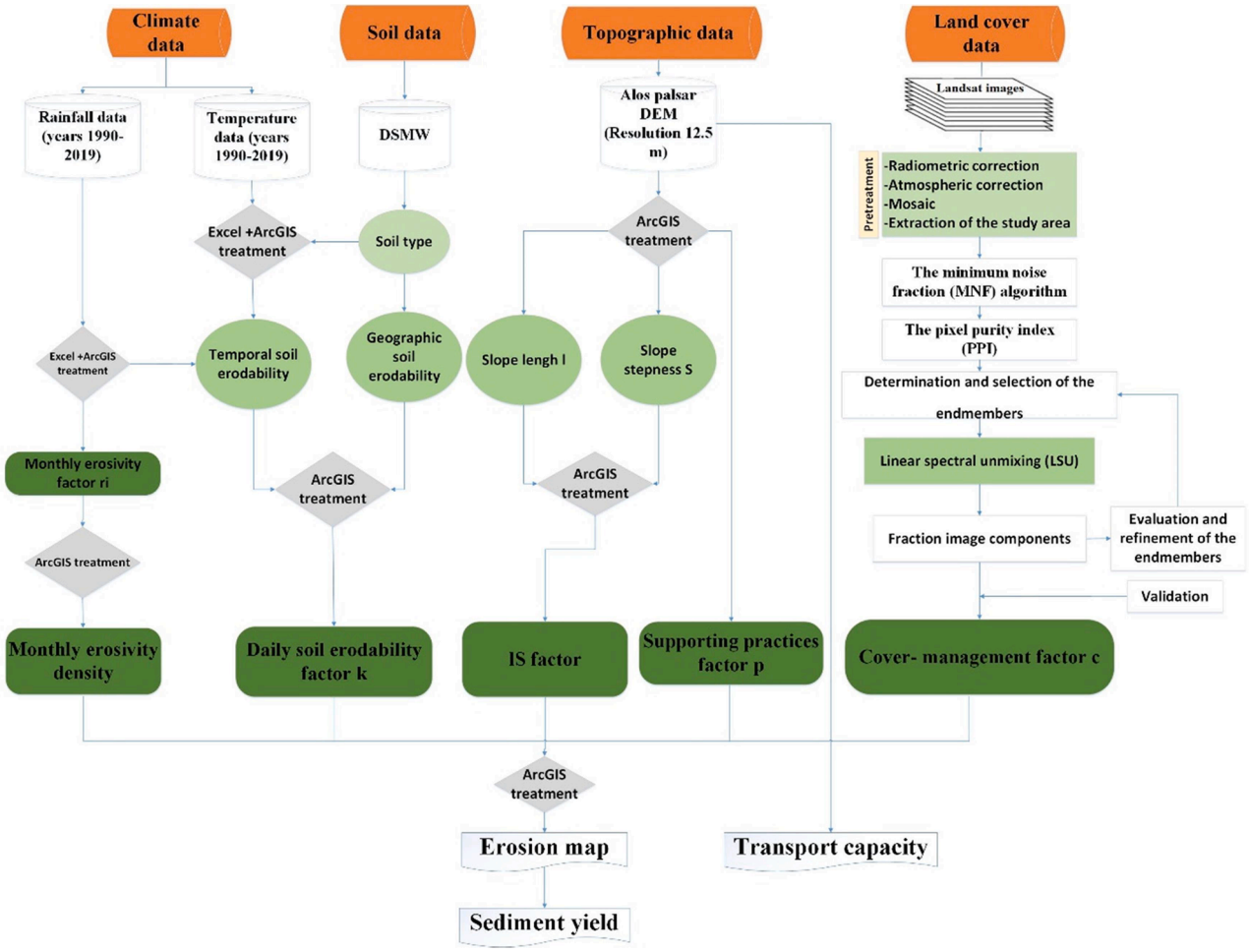

Fig. 2. Flowchart of the RUSLE2-LSU methodology.

Wen, 2013; Paul M. Mather and Koch, 2011).

3.1.2. *Improvement of the soil erodibility K factor*

The improved soil erodibility estimate comprises a geographical and temporal component affected by variations in temperature. The spatial variation in precipitation and temperature should be integrated as input in the soil erodibility equation to improve soil erodibility K factor estimation.

3.1.2.1. Estimation of the K factor using temperature data. In the present study, the effect of past climate change on soil erodibility K was observed in the temporal K factors. As temperature and precipitation vary with location, soil erodibility factor values also vary with location (Renard et al., 1997). The equations used to compute the temporal soil erodibility for summer conditions (USDA-ARS, 2013) are as follows:

$$\frac{K_i}{K_w} = 0.591 + 0.732\left(\frac{P_i}{P_s}\right) - 0.324\left(\frac{T_i}{T_s}\right) \quad \mathrm{Tj} \geq 40^{\circ}\ \mathrm{F} \tag{3}$$

if $\frac{K_i}{K_w} > 2$, then $\frac{K_i}{K_w} = 2$

if $\frac{K_i}{K_w} < 0{,}4$, then $\frac{K_i}{K_w} = 0.4$where K_i represents the average daily soil erodibility factor for the ith day; K_w denotes soil erodibility value from the RUSLE2 soil erodibility nomograph, T_i denotes average daily temperature for the ith day (^{o}F), T_s represents average temperature for the summer period, P_i denotes average daily precipitation, and P_s represents average precipitation for the summer period.

An upper limit of 2 and a lower limit of 0.4 for the ratio $\frac{K_i}{K_w}$ provides robustness by preventing effects of extreme precipitation and temperature and by reducing the chances of obtaining excessive daily soil erodibility values (USDA-ARS, 2013).

3.1.2.2. Estimation of the geographical K factor. The geographical K-factor was estimated using Wischmeier's nomograph (Renard et al., 1997) and has been expressed as follows:

$$K = \frac{2.1{*}10^{-4}{*}M^{1.14}(12 - OM) + 3.25(2 - b) + 2.5(c - 3)}{759} \tag{4}$$

where M is calculated as (percentage Limons + percentage very fine sands) × (100% clay); OM indicates percentage inherent soil organic matter; b denotes structure code; and c represents profile permeability code.

The distinction between this equation and the USLE and RUSLE equivalent equation in the standard soil erodibility nomograph is the algebraic sign of b (USDA-ARS, 2013). Data of all geographical soil erodibility factors were corrected according to the findings presented in field studies (Roose, 1977).

3.1.3. *Estimation of monthly erosivity density*

Various approaches have been used to estimate the R-factor (Benavidez et al., 2018; Yin et al., 2017). Roose, while working on the R-factor in West Africa, reported the existence of a simple relationship between the average annual R and the average annual rainfall erosion (Roose, 1975; Roose, 1977). However, Roose's equation does not consider data on daily rainfall. As RUSLE2 application is based on the consideration of daily values of erosivity, precipitation, and temperature to compute erosion, we considered the relationship reported by Wischmeier and

Smith (1978) and which was later modified by Arnoldus (1980). This equation is best suited for investigation of study areas that lack high temporal resolution rainfall records and incorporates monthly and annual rainfall values (Vijith et al., 2017). This equation demonstrates the advantage being used for estimating monthly rainfall erosivity. In the present study, the R-factor was computed using annual and monthly rainfall data because of the lack of availability of data in the Boubo watershed. We used Wischmeier and Smith (1978) equation, which was later modified by Arnoldus (1980):

$$R = \sum_{i=1}^{12} 1.735 * 10^{\left[1.5 log_{10}\left(\frac{P_i^2}{P}\right) - 0.08188\right]} \quad (5)$$

where R represents the erosivity factor (MJ mm $ha^{-1}h^{-1}$ $year^{-1}$), P_i denotes the monthly precipitation (mm), and P represents the annual precipitation (mm).

The monthly erosivity density is the preferred new method input for climate data in RUSLE2 (McCool and Yoder, 2004). RUSLE2 computes monthly erosivity by multiplying the monthly erosivity density by monthly precipitation (USDA-ARS, 2008) as follows:

$$R_e = \alpha_e P_e \quad (6)$$

where R_e represents the monthly erosivity, α_e denotes the monthly erosivity density, and P_e represents the monthly precipitation.

We used the kriging method to generate a spatial interpolation map of the monthly erosivity and monthly erosivity density.

3.1.4. Estimation of slope length L factor

Various LS factors have been developed (Ghosal and Das Bhattacharya, 2020; Hrabalíková and Janeček, 2017). In GIS-based studies, slope steepness is not uniform for the entire area, and this results in the sub-division of the slope into several segments (Foster and Wischmeier, 1974). Desmet and Govers (1996) extended this approach to two-dimensional terrain using the concept of the unit-contributing area. Previous studies only considered the steepness of the slope exponent m; however, the latest approach demonstrates the advantage of incorporating data on the flow path steepness, soil, and cover management in the equation of the slope exponent. The L factor was calculated using the expressions reported in a previous study (Desmet and Govers, 1996) as follows:

$$L_{i,j} = \frac{\left(A_{i,j-in} + D^2\right)^{m+1} - A_{i,j-in}^{m+1}}{D^{m+2} * x_{i,j}^m * 22,13^m} \quad (7)$$

$$m = \frac{\beta}{(\beta + 1)} \quad (8)$$

$$\beta = \left[\frac{k_r}{k_i}\right]\left[\frac{c_r}{c_i}\right]\left[\frac{exp(-0.05 f_g)}{exp(-0.025 f_g)}\right]\left[\frac{(sin\theta/0.0896)}{3(sin\theta)^{0.8} + 0.56}\right] \quad (9)$$

where $L_{i,j}$ denotes the slope length factor for the ith segment; D represents the grid cell size (m); $X_{i,j}$ is calculated as sin $a_{i,j}$ + cos $a_{i,j}$; $A_{i,j}$ denotes aspect direction the grid cell with coordinates (i,j); A represents flow accumulation at the intlet of a grid cell (m^2), m denotes the slope length factor exponent according to β, and β represents the erosion ratio in rill to interill erosion; additionally, $\left[\frac{k_r}{k_i}\right]$ denotes rill erodibility to interrill erodibility ratio, and is calculated as follows:

$$\frac{K_r}{K_i} = \left(\frac{P_{sd}}{100}\right)\left[(1 - exp(-0,05P_{sd}))\right] + 2,7\left(\frac{P_{sl}}{100}\right)^{2,5}\left[1 - exp(-0,05P_{sl})\right] + 0,35\left(\frac{P_{cl}}{100}\right)\left[1 - exp(-0,005P_{cl})\right] \quad (10)$$

where $\left[\frac{c_r}{c_i}\right]$ = ratio of below-ground effects for rill and interill erosion; $\left[\frac{exp(-0.05 f_g)}{exp(-0.025 f_g)}\right]$ = ratio of ground cover effects on rill and interill erosion; $\left[\frac{(sin\theta/0.0896)}{3(sin\theta)^{0.8} + 0.56}\right]$ = ratio of slope effects for rill and interrill erosion; θ represents slope steepness angle; and fg denotes percentage of ground cover.

3.1.5. Estimation of the S and P factor

The equation of the invariant steepness relationship is described (USDA-ARS, 2013) as follows:

$$S = 10.8s + 0.03 \quad S_p < 9\% \quad (11)$$

$$S = 16.8s + 0.5 \quad S_p \geq 9\% \quad (12)$$

where S denotes the steepness factor (nondimensional), s represents the sine of the slope angle, and s_p is equal to a value that is 100 times the tangent of the slope angle.

Changes in support practices, such as contour tillage and terracing, cannot be represented via land use maps at large watershed scales (Alemaw et al., 2013; C. et al., 2011; M. et al., 2016). In this case, we used another method to estimate the p factor based on slope gradients used as inputs, as reported by Wenner. The equation put forth by Wenner (1980) is expressed as follows:

$$p = 0.2 + 0.3 * S \quad (13)$$

where S denotes the slope grade in percent (%).

3.2. The estimation of the sediment transport capacity and sediment yield

The sediment transport capacity and sediment yield are deemed two outputs of the RUSLE2 model and are considered essential variables for providing guidance to managers for the adoption of adequate regional policies.

3.2.1. Sediment transport capacity

When using GIS to estimate the spatial change in erosion and deposition over the landscape in a soil erosion model, sediment transport capacity must be considered (Wang et al., 2015). Different types of and equations for transport capacity relationships are used in physically based sediment transport studies (Hajigholizadeh et al., 2018; Her, 2011; Kothyari et al., 2002; Merritt et al., 2003; Papanicolaou et al., 2008; Wang et al., 2019). More recently, machine learning has been applied to estimate sediment transport (Alizadeh et al., 2017; Chen and Chau, 2019; Reisenbüchler et al., 2021; Sharafati et al., 2020). However, it is necessary to use a sufficiently large and diverse database from the training site to develop a general and applicable method. Studies have demonstrated that machine learning does not provide good results because of data limitations (Li et al., 2016). We used the simple equation in RUSLE2 because of the difficulties in environmental modeling characterized by problems of natural complexity, spatial heterogeneity, and the lack of availability of data. The sediment transport capacity of runoff in rill areas is (USDA-ARS, 2013) expressed as follows:

$$T_c = K_T q s \quad (14)$$

where the RUSLE2 coefficient K_T for sediment transportability is represented as K_T = 4004.62 t/m^3, described by RUSLE2 Science Documentation (USDA-ARS, 2013), and s denotes the sin of the slope angle (dimensionless).

The rainfall-runoff generation procedure is extremely complex (Cristiano et al., 2017). We estimated the runoff rate as a function of the drainage surface, runoff coefficient, and mean precipitation using a

rational formula (Asare-Kyei et al., 2015)

This equation is expressed as follows:

$$q = kPA \tag{15}$$

where q represents runoff (m^3), k denotes the runoff coefficient, P represents the average rainfall (mm), and A denotes the drainage area (m^2).

3.2.2. Sediment yield (SY) / sediment delivery ratio (SDR)

When integrating RUSLE2 and GIS, selection of representative profiles may be problematic (Dabney et al., 2015). In relatively large watersheds, the majority of sediment is deposited inside the watershed, and only a small percentage of soil eroded from hillslopes reaches the stream and watershed outlet (Ebrahimzadeh et al., 2018; Lim et al., 2005). In erosion and sedimentation research, understanding the sediment delivery process at the watershed scale remains challenging. Various models have been developed to estimate the sediment delivery ratio (SDR) based on the area power function and drainage area (Renfro, 1975; USDA, 1983; Vanoni, 1975), rainfall-runoff factors (Arnold et al., 1998), slope gradient (Williams and Brendt, 1972), relief-length ratio (Maner, 1958), particle size (Walling, 1983), water runoff travel time (Ferro, 1997; Ferro and Minacapilli, 1995; Ferro et al., 1998), distance-slope (Sun and McNulty, 1998), and runoff curve numbers (Williams, 1977). Progress in SDR has been witnessed in several studies (Wu et al., 2017). To accurately estimate the sediment yield in a watershed, it is advised to use watershed-specific SDR curves; however, the obtainment of a specific SDR curve is not easy (Lim et al., 2005). It was challenging to select the most suitable SDR model in this study area, mainly because of the lack of investigations of this approach using observed data derived from this area. However, studies have demonstrated that Maner's equation, and William and Berndt's equation perform well in tropical watersheds (Colman et al., 2018). Hamontree et al. (2018) noted that consideration of Maner's equation showed better results than that observed with William and Berndt's equation. The SDR was used to estimate the sediment yield. The SDR formula used in this study (Maner, 1958) is expressed as follows:

$$\log(SDR) = 2.94 + 0.82\log\frac{R}{L} \tag{16}$$

where SDR denotes the sediment delivery ratio, R represents the relief of the watershed, and L represents the maximum length of the watershed.

Using the SDR value derived from Eq. (16), SY can be estimated using the equation proposed by (Wischmeier and Smith, 1978) as follows:

$$SY = SDR \times E \tag{17}$$

where SY denotes the sediment yield (ton/ha/yr) and E represents the annual potential soil loss (ton/ha/yr); in the present study, we assumed that gross erosion (E) was only rill and interill erosion (A) and was estimated via RUSLE2.

4. Results

4.1. Mapping of the cover management with LSU

The variation in cover management using LSU is presented in Fig. 3. Cover management was estimated using Eq. (2). The pixel-by-pixel method of LSU was selected and appreciable results were obtained for the large Boubo watershed. The average of the root-mean-squared errors (RMSE) for the whole image of LSU was 0.46 in 1990 and was 0.26 in

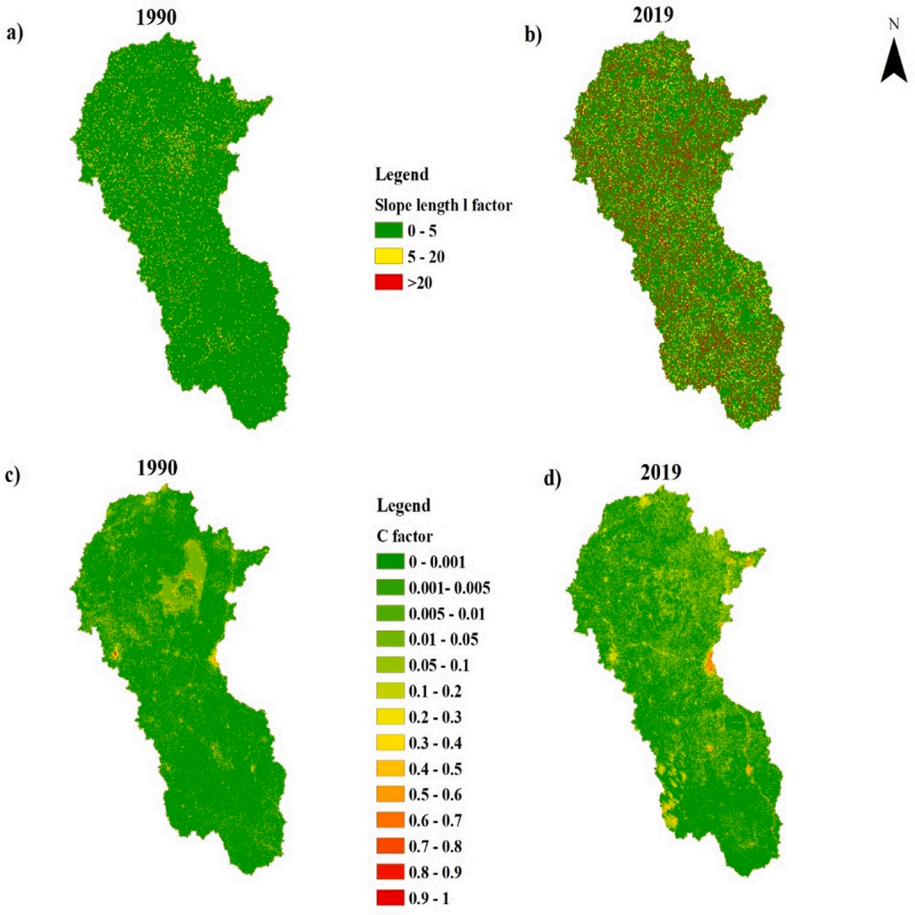

Fig. 3. a) Slope length factor in 1990; b) slope length factor in 2019; c) cover management in 1990; and d) cover management in 1990.

2019. This small value indicates good selection of endmembers, sufficiency, and validity. Based on the available data, this is a reliable method for estimating the C factor. Cover management results show that 84.66% and 73.31% of the study area had vegetation cover in 1990 and 2019, respectively. Changes in cover management for different crops exhibit a significant influence on soil loss (Fig. 3).

4.2. Improved soil erodibility K factor

4.2.1. Estimation of the geographical K factor

Four different geographical K-values were obtained using Eq. (4) and were corrected to k = 0.1. Table 3 summarizes the textural classes of the Boubo watershed. A map of the geographical soil erodibility factor is depicted in Fig. 7.

4.2.2. Estimation of the K factor using temperature data

The effect of temperature in the soil erodibility K factor was estimated using Eq. (3). The graph in Fig. 4 shows the variation in the mean temporal K value during the years 1990 and 2019. Fig. 5 and Fig. 6 represent the map of the effect of temperature on the variation in the temporal soil erodibility K factor.

Different patterns of temporal variation in K were observed, with the observation of a general increase in variation over time. October presented with the highest change, with an increase in K of up to 107.86% (Fig. 4). In October, the increasing K value indicates the manner in which temperature and precipitation change during the rainy season in the watershed and impact erosion. In October, precipitation increased by 58.16% and temperature decreased by 1.04% from 1990 to 2019. Temporal K was the highest in May 1990 (0.194) and was the highest in June 2019 (0.2).

4.3. Estimation of S and P factors

The P factor value was estimated using Eq. (13). On the slope between 0% and 5%, the mean P factor was 0.88. Our study showed that 80.22% of the Boubo watershed presented with a P factor ranging between 0.93 and 1. This suggests that topographic features affect erosion. The map shows that the P factor value is associated with topographical characteristics and the value is high in the entire watershed. The slope leads to a spatial change in the P factor at the watershed scale (Fig. 7).

4.4. Impact of climate change on erosion

Fig. 8 illustrates the variation in precipitation and temperature in the Boubo coastal watershed from 1990 to 2019. The Boubo watershed presented high climate variability over the indicated years.

The monthly erosivity factor was estimated using Eq. (5) and the value was then integrated with Eq. (6) to obtain the monthly erosivity density. The value of the monthly erosivity density in the Boubo watershed over different months varied between 0.05 and 20.86 in 1990 and ranged from 0.8 to 21.21 in 2019 (Figs. 9 and 10).

Different trends helped characterize the variations in the monthly rainfall and erosivity density values between 2019 and 1990. March demonstrated the highest change, with an increase in monthly rainfall erosivity density of up to 908.55%, varying from 0.2 in 1990 to 2.06% in 2019 (Fig. 11). During the rainy season, Boubo experienced the heaviest rainfall of the year. In January, February, March, July, August, and October, increasing monthly rainfall erosivity density was observed. In June, the R factor increased by 0.97% from 1990 to 2019, but the June erosivity density decreased by 4.38%. These observations were attributable to the high variation in precipitation. In both years, June presented with the highest erosion density, although a less remarkable difference in variability was observed for this month. The Pearson correlation showed statistically significant positive correlations between the average monthly precipitation and the monthly erosivity density in each period ($p < 0.05$), $R = 0.964$ in 1990, and $R = 0.978$ in 2019.

Six potential erosion classes were used for generation of the map to represent the relative monthly soil loss, varying from slight to very severe. Most areas with high potential erodibility depicted on the map in Figs. 12 and 13 were cultivated or settlement areas.

Soil loss varied significantly in March and October (rainy season) from 1990 to 2019 (Fig. 14). Soil loss was considerable in June and damaged most surface in the Boubo watershed. In June, the mean soil loss rate was 0.048 t/ha/month in 1990 and was 0.073 t/ha/month in 2019. High erosion rates could be observed around the cities of Divo, Diegonefla, and Guitry (Figs. 12 and 13). In January, February, March, June, July, September, and October, accelerated soil erosion was observed for the years 1990 to 2019 (Fig. 14).

4.5. Sediment transport capacity (Tc) and sediment yield (SY)

The sediment transport capacity notably increased as the climate conditions changed over the year (Fig. 15). The results obtained suggest that it is possible to predict the sediment transport capacity using GIS and the simple empirical relationship proposed by RUSLE2.

A previous incidence of climate change significantly impacts the sediment yield. The sediment yield increased by 133.02% from 1990 to 2019 (Table 4). Table 4 displays the numerical results for the soil erosion and sediment yield in the Boubo watershed.

5. Discussion

This is the first study conducted on the assessment of the impacts of long-term climate and vegetation changes on soil erosion and sediment yield in the Boubo coastal watershed. The main goal of this study was to combine RUSLE2 and LSU to assess the impacts of climate and vegetation cover changes on soil erosion and sediment yield.

Climate data, vegetation cover information, and soil characteristics are essential for soil erosion modeling. The approximation of rainfall erosivity density and the improved soil erodibility K factor depend on the climate data. However, few direct field measurements on soil loss and sedimentation in the Boubo coastal watershed are available, and the existing data derived from the Divo station are old and cannot be used to represent the overall watershed (Roose, 1983; Roose, 1996). In Côte

Table 3
Soil-textural class data for the Boubo watershed.

Soil ID	Soil texture	Hydrologic soil group	Permeability code	Rill to interill soil erodability ratio K_r/K_i (source: USDA 2013)	K factor (t.ha.h.ha^{-1}.MJ^{-1}.mm^{-1})	Areas	
						Km^2	%
Bf- Ferralic Cambisols	Clay	D	6	0.36	0.022	1496	29.63
Af-Ferric Acrisols	Sandy clay loam	C	4	0.65	0.020	2594.03	51.38
Ao-Orthic Acrisols	Sandy clay loam	C	4	0.65	0.018	859.98	17.04
Fx- Xanthic Ferralsols	Sandy clay	D	2	0.61	0.008	98.26	1.95
Total						5048.27	100

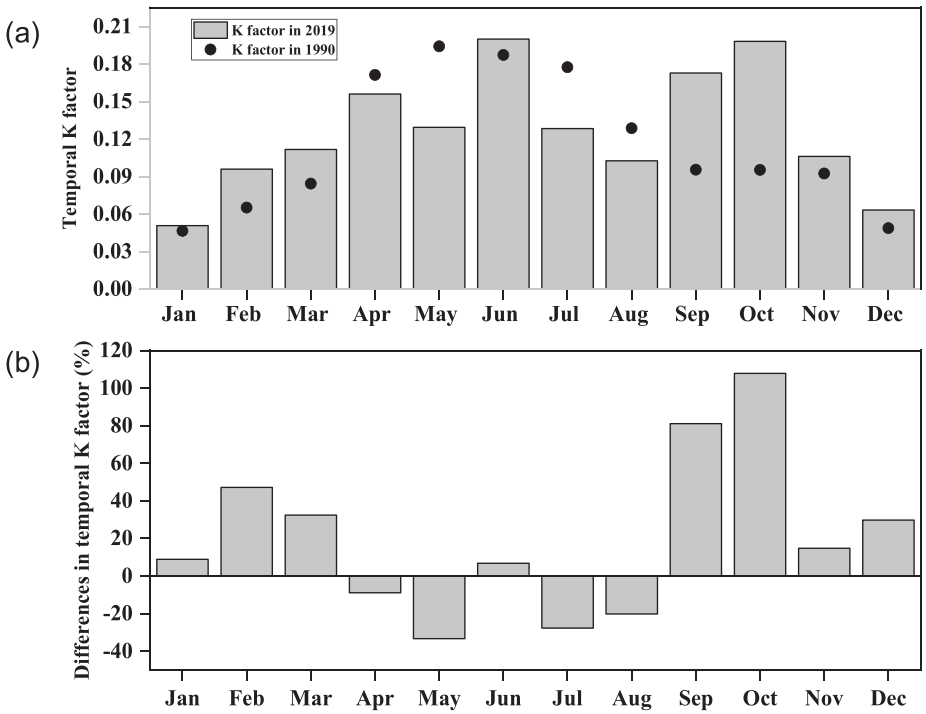

Fig. 4. (a): Comparison of the mean temporal K factor during the year 1990 and 2019; (b): difference (%) in average temporal soil erodibility in 1990 and 2019.

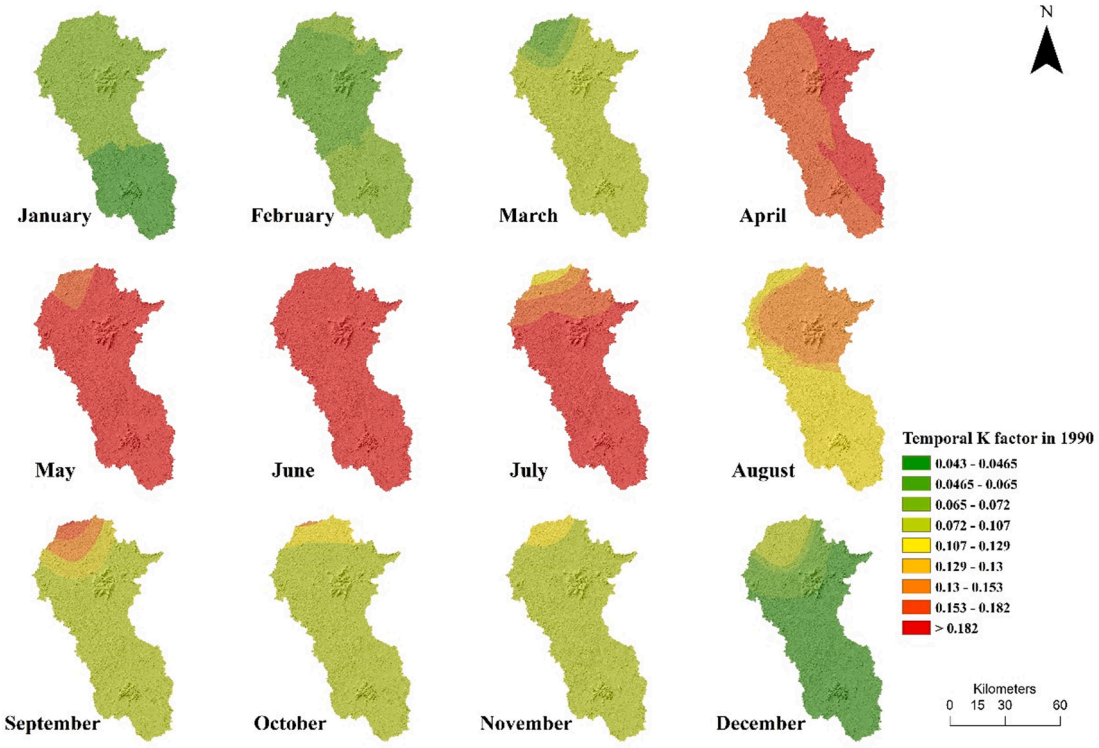

Fig. 5. Temperature effect on the variation in soil erodibility in 1990.

d'Ivoire, soil erosion is a neglected problem, resulting in a lack of long-term data collection. The incomplete preparedness of Côte d'Ivoire to tackle global climate change explains its high vulnerability (Worldbank, 2018). Similar studies have noted that soil erosion is a grave issue worldwide, but it is sometimes neglected (Garcia-Ruiz et al., 2016), and a lack of data collection has been noted in Africa (Borrelli et al., 2021; Lal, 2009; Vanmaercke et al., 2014). Modeling of soil erosion and sediment yield in areas where data are missing is challenging. Fortunately, remote sensing and GIS enable the study of the long-term impact of land cover change on soil erosion for ecological management in this area. In Africa, satellite images are considered excellent tools for mapping waterborne erosion at the watershed scale (Vrieling et al., 2010). Therefore, we used data available on the Internet to achieve our goal. The new approach of combining RULE2 and LSU contributes not only to

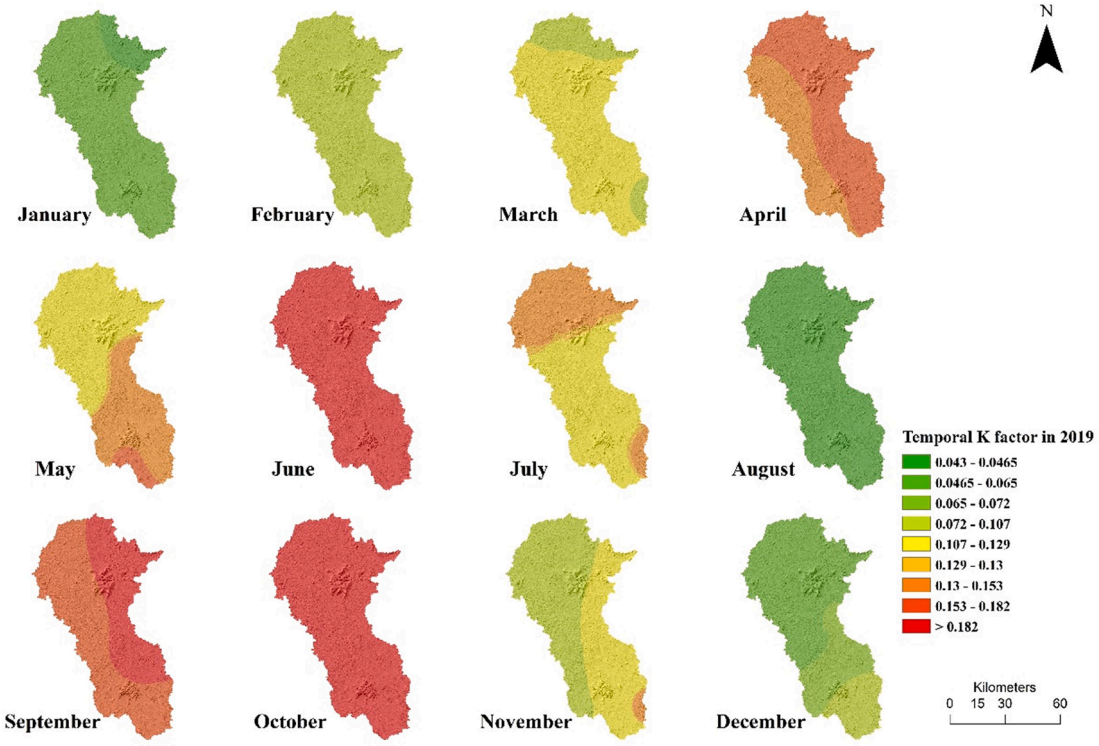

Fig. 6. Temperature effect on the variation in soil erodibility in 2019.

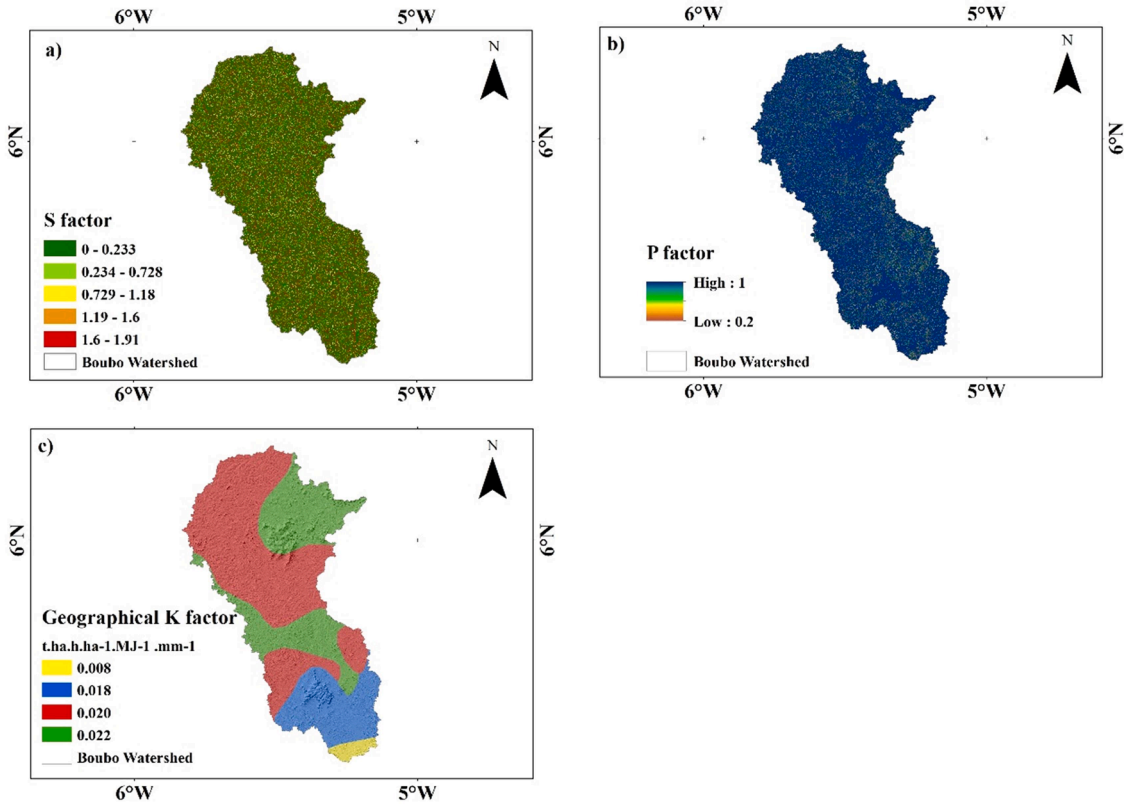

Fig. 7. a) Slope steepness factor; b) support practices map; and c) geographical soil erodibility map.

the debate of modeling erosion at the pixel level, but also reveals the negative impact of climate change and human activities around the cities of Divo, Diegonefla, Guitry, and Lakota. Similar studies in several Ivorian coastal watersheds have revealed that human activities impact soil loss, runoff, and sedimentation (Kouadio, 2011; Sébastien et al., 2013). To improve the field data limitation of this study, an integrated

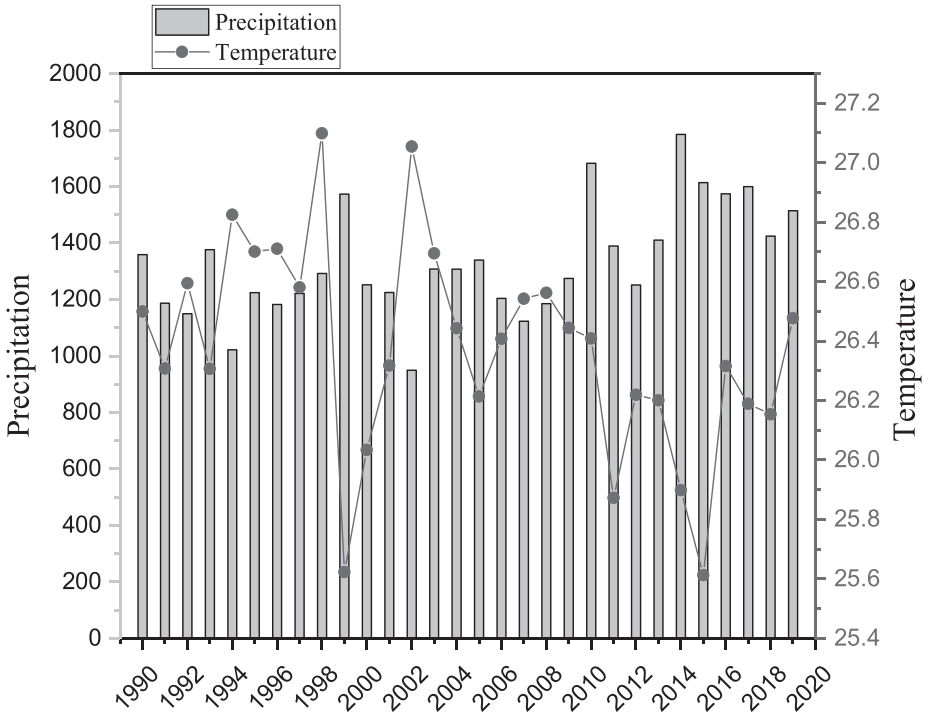

Fig. 8. Annual average rainfall and temperature over a period of 29 years (1990–2019).

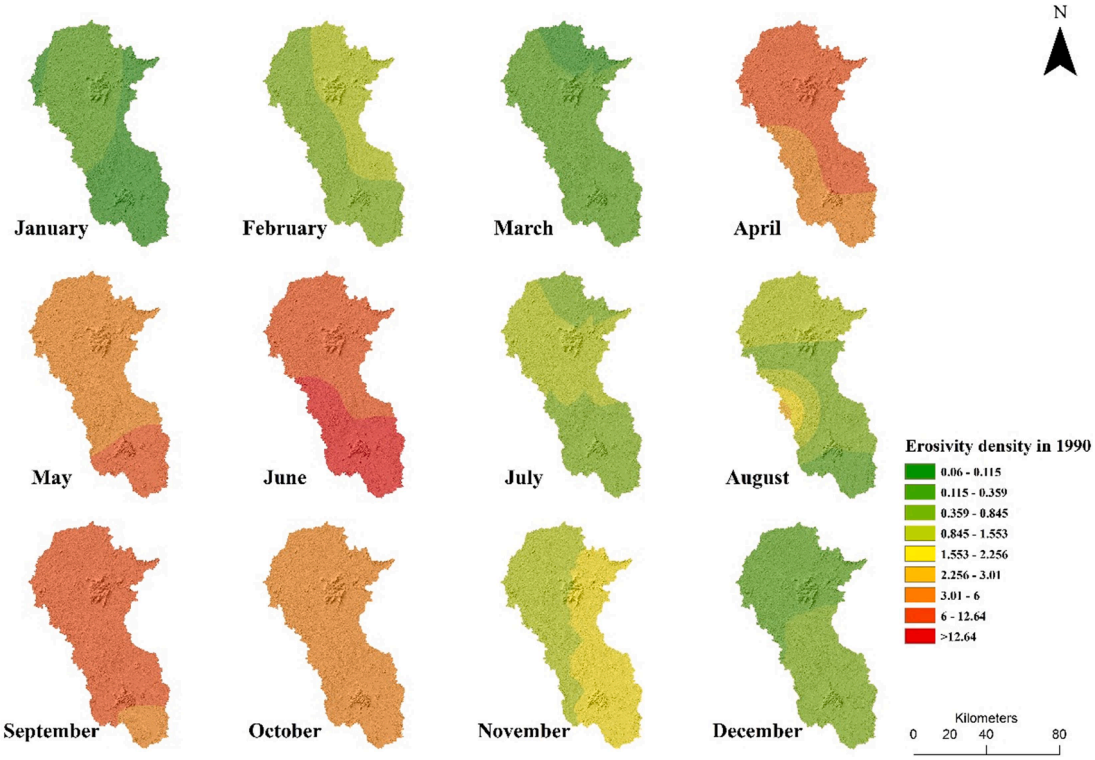

Fig. 9. Spatiotemporal variation in the monthly erosivity density for the year 1990.

platform for sharing data in an open access format is necessary to create a strong community of researchers to better understand soil erosion and sedimentation in all countries, specifically in the Boubo watershed. Similarly, Panagos and Katsoyiannis (2019) proposed the integration and sharing of data with other soil-related disciplines.

Our study revealed accelerated soil loss from 1990 to 2019. The dynamics of LULC observed in the Boubo watershed negatively impact both environment and ecological conditions. The most considerable environmental and ecological problems in the Boubo watershed include the exploitation of forest resources for agriculture and construction purposes. This exploitation is attributable to development planning that focuses on establishing and improving Côte d'Ivoire's economy based on

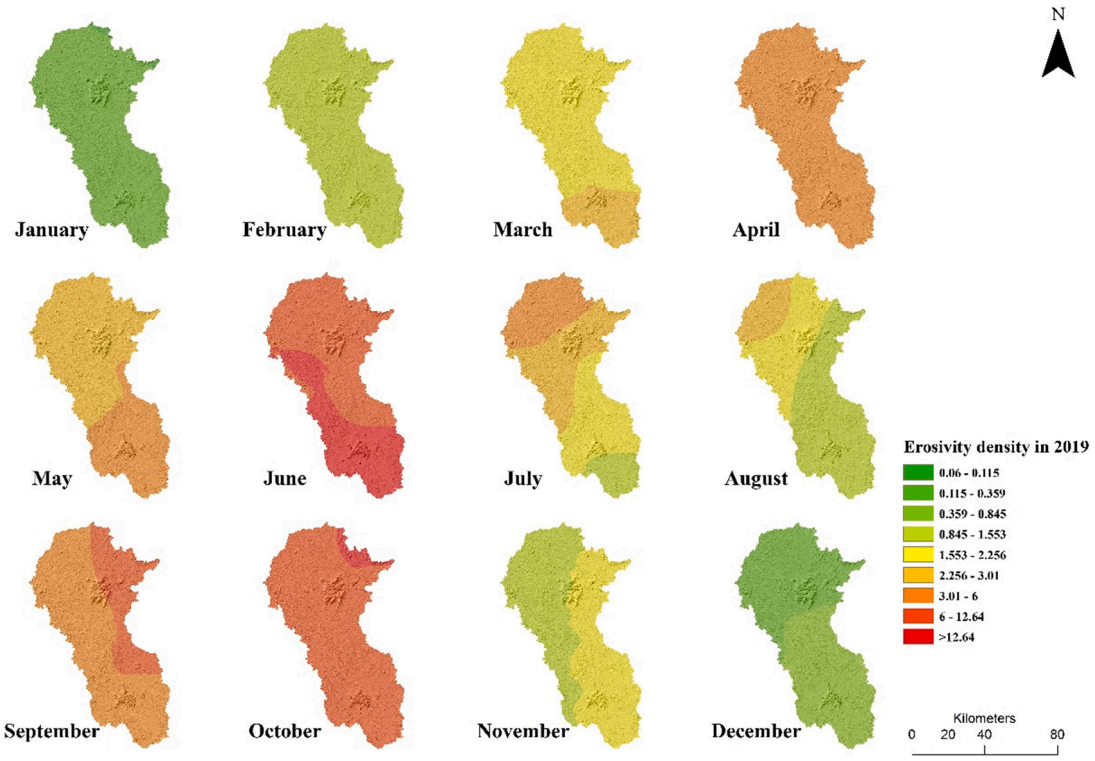

Fig. 10. Spatiotemporal variation in the monthly erosivity density for the year 2019.

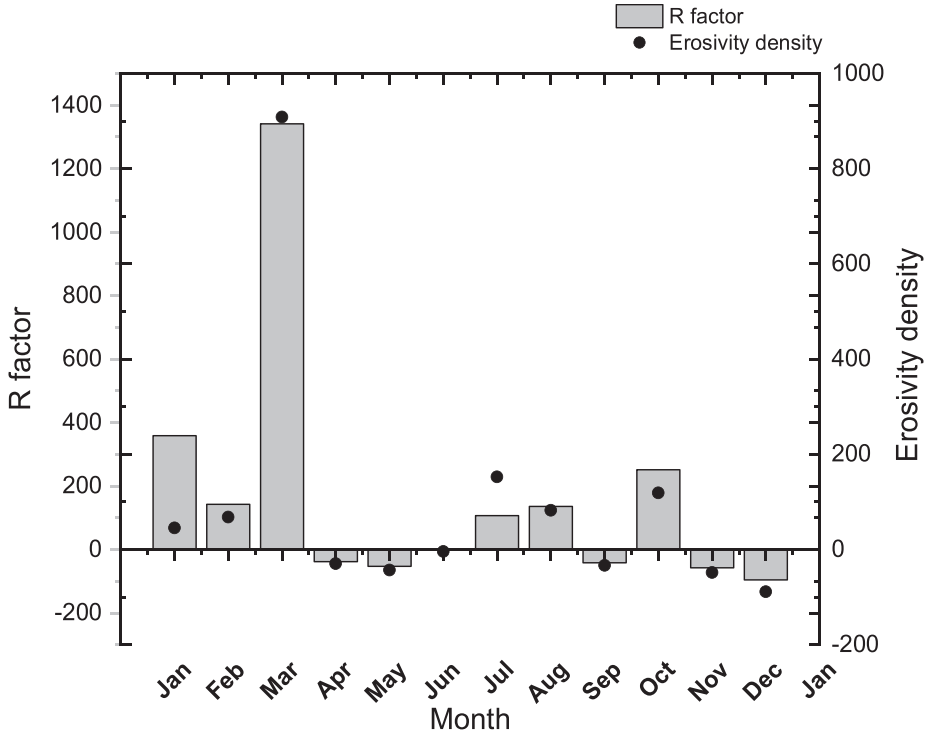

Fig. 11. Differences (%) between the monthly R factor and monthly density erosivity from 1990 to 2019.

agricultural practices. The European Space Agency land cover classification showed a deforestation rate of over 65.49% from 1992 to 2019 in the Boubo coastal watershed. Deforested lands are exposed to the potential impacts of raindrops, which accelerate the detachment, removal, and transportation of soil particles. The importance of the change in the Boubo watershed (increase in agricultural land and urban areas) and the variation in the C factor proves that the exposure of the surface of the watershed favors an increased frequency of erosion phenomena. Similar changes have been recorded in Côte d'Ivoire (ONU-REDD+, 2017). Côte d'Ivoire presents with one of the highest deforestation rates in West Africa. Over the last 50 years, the country has lost nearly 80% of its natural forests due to the extension of uncontrolled agricultural surfaces

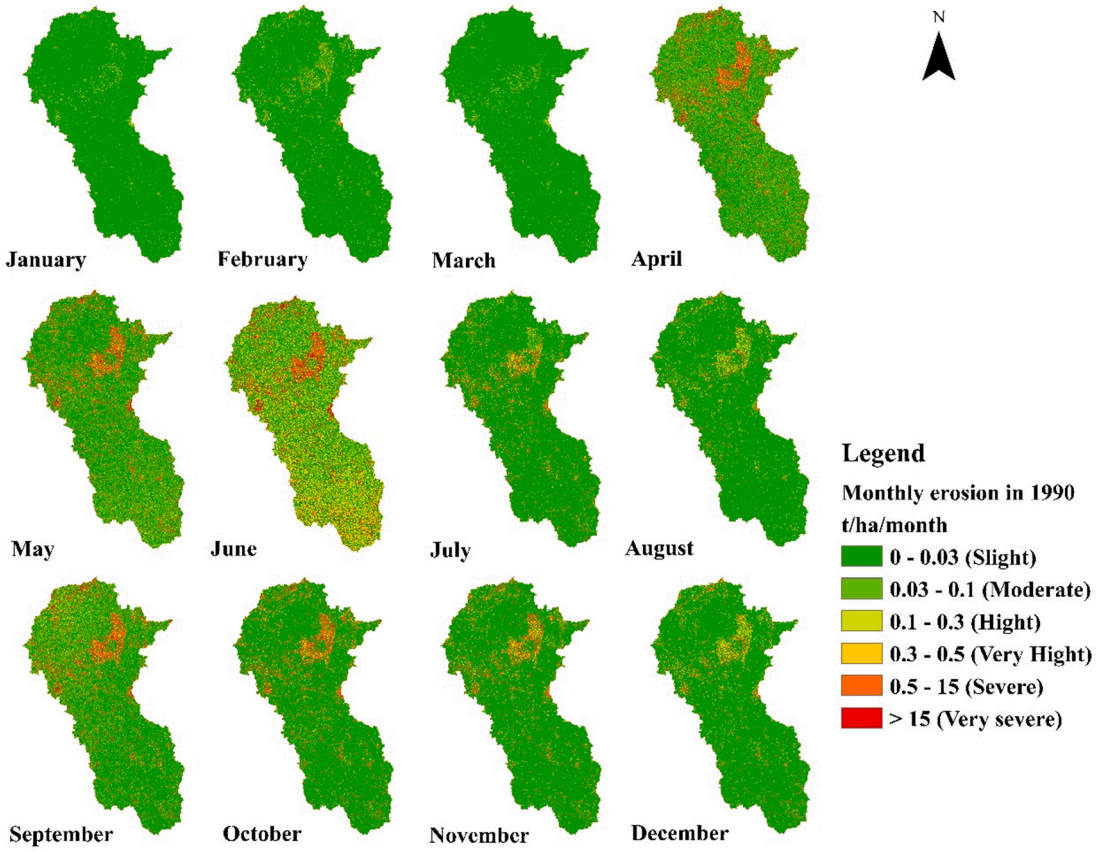

Fig. 12. Soil erosion during the year 1990.

(M.E.D.D., 2019; REDD+, 2018). In the Boubo watershed, degradation of forest landscapes directly affects soil productivity. Recently, the Restoration Opportunities Assessment Methodology (ROAM) was implemented in Côte d'Ivoire to identify drivers of forest degradation and to map restoration priorities (IUCN, 2016). Our study showed that change in vegetation cover exerts an effect on soil loss in the Boubo coastal watershed. Therefore, modeling of soil erosion using GIS should be performed by considering mixed land cover patterns to better identify potential erosion areas. Therefore, we used LSU in the Boubo watershed. Recent studies have used LSU and reported satisfactory results (De Asis and Omasa, 2007; De Asis et al., 2008; Ma et al., 2010; Meusburger et al., 2010b; Schmidt et al., 2018). Researchers have used geostatistical methods (Wang et al., 2002) and machine learning techniques (Tsai et al., 2021) to improve and map the C factor; however, implementation of such a method in the study area is challenging. Further studies with more accurate data should be conducted to explore applications of LSU, geostatistical simulation, and the machine learning approach to evaluate the best method for representing the spatial variability in the C factor in this area. Reforestation and the association of culture with good green cover may be deemed a good measure to mitigate soil loss. A similar approach has been used to reduce soil loss by 98% in other areas in Côte d'Ivoire (Koua et al., 2019). Additional ecosystem service research is lacking for Côte d'Ivoire (Wangai et al., 2016). Ecosystem management based on ecosystem services and sediment deposition potential may be considered an excellent approach to mitigate soil degradation and to increase soil productivity in the study area. Other researchers have proposed the consideration of such an approach (Syrbe et al., 2018).

This study shows that there are four types of soils (Ferralic Cambisols, Ferric Acrisols, Orthic Acrisols, and Xanthic Ferralsols) in the Boubo watershed. One major improvement of RUSLE2 is the integration of the effect of climate in the estimation of the K factor. This study shows that the temporal soil erodibility changes with precipitation and temperature variations in the Boubo watershed. Geographical K factor values correspond to those reported by Roose (1996) (K varies from 0.01 to 0.7). Our research shows that the influence of temperature on soil erodibility is significant. Similarly, Kinnell (2019) demonstrated that climate change could exert an effect on soil erodibility. In this study, we used kriging for spatial interpolation because a geostatistical analysis of the K factor indicated better spatial representation than that observed with the traditional method (Baskan and Dengiz, 2008). Previous authors used a similar geostatistical approach to estimate the K factor (Ferreira and Panagopoulos, 2014). Future studies should consider climate change using more accurate data and geostatistical methods to better represent soil erodibility.

The spatial distribution of the monthly erosivity density showed that the watershed was subjected to rain aggressiveness. The estimation reveals that the rainfall erosivity density exhibits a high year-to-year variability. In June, the R factor increased by 0.97% from 1990 to 2019, but the June erosivity density decreased by 4.38%. Increasing precipitation in June tends to reduce the June erosivity density because of the precipitation position in Eq. (6). When precipitation increased, the monthly erosivity density decreased. Similar trends between rainfall erosivity and rainfall erosivity density have been noted and mapped in other areas (Ballabio et al., 2017; Panagos et al., 2016; Schmidt et al., 2016). Occasional rainstorms are extremely powerful and erosive. Similarly, in the Ivory Coast, Brunet-Moret (1967) and Roose (1996) have noted that climatic erosivity is extremely high in humid tropics, presenting with rains that are twenty to hundred times more erosive than those reported in temperate areas, two times more erosive than those in tropical environments, and five times more aggressive than those in Mediterranean environments. Further research in the study area should be conducted to update Roose's estimation of the R factor to that of the monthly erosivity for better estimation because the new RUSLE2

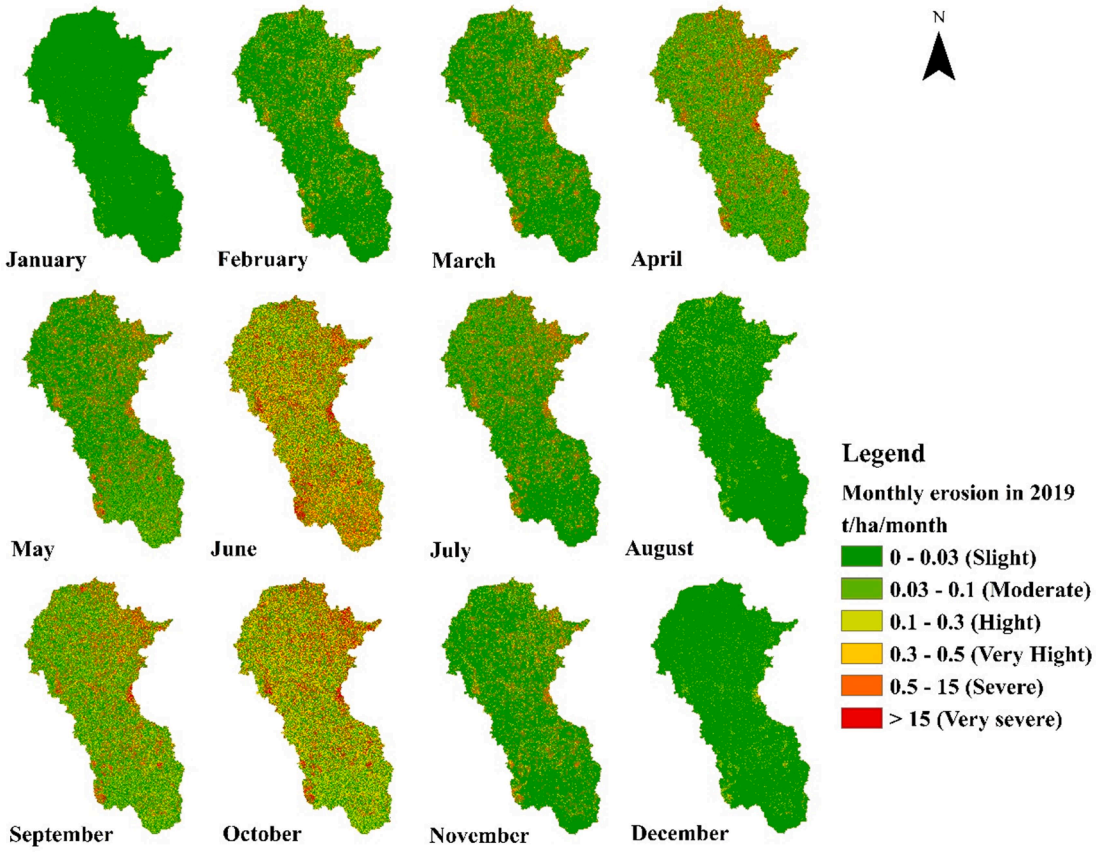

Fig. 13. Soil erosion during the year 2019.

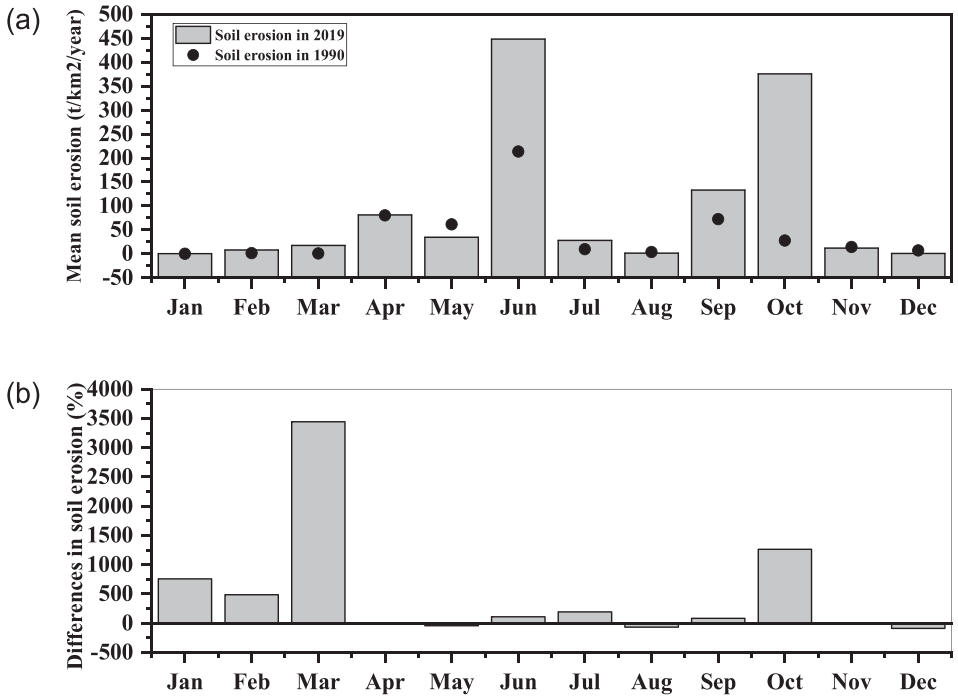

Fig. 14. (a): Comparison of soil erosion during 1990 and 2019; (b): difference (%) in average soil erosion in 1990 and 2019.

concept of monthly erosivity density may help improve the mapping of rainfall erosivity. Recent studies have indicated that consideration of the monthly erosivity density provides good results in the United States (Yin et al., 2017). During April, May, June, September, and October in 1990, and in the northern part of Diegonefla in July 2019, the monthly erosivity density was extremely high in the Boubo coastal watershed.

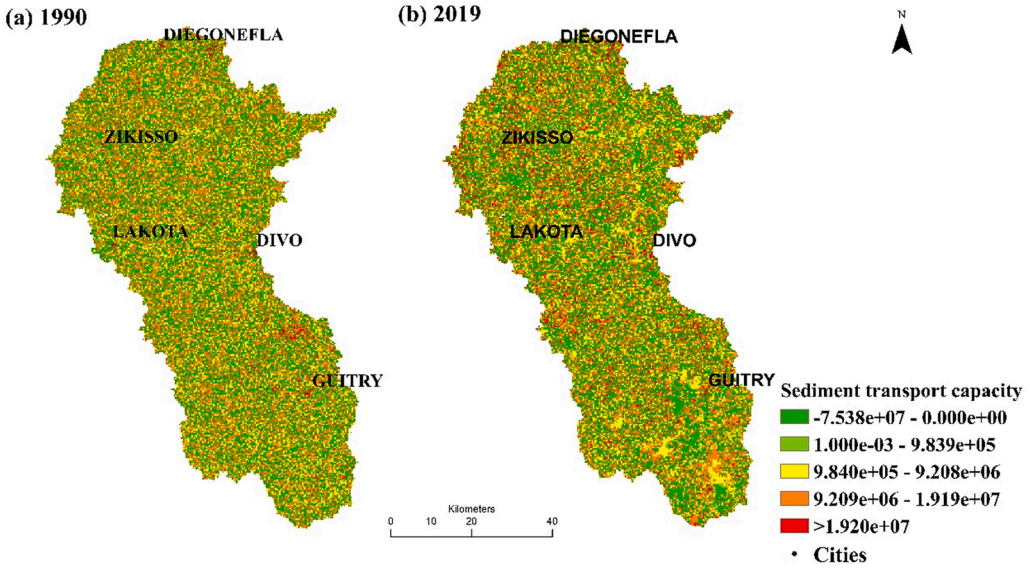

Fig. 15. Variation in the sediment transport capacity from 1990 to 2019.

Table 4
Soil erosion rate and sediment yield in the Boubo watershed.

Year	Average rate of soil loss (t/ha/yr)	Total extent of soil loss for the watershed (t/yr)	Average value of SDR	Average rate of sediment yield (t/ha/yr)	Total extent of sediment yield in the watershed (t/yr)
1990	0.41	20.64	2.67	1.09	55.11
2019	0.95	47.95	2.67	2.54	128.04

This study revealed a high soil erosion rate during the indicated periods. This implies that the monthly erosivity density considerably contributes to higher runoff and soil loss predictions. Similarly, according to Dabney et al. (2011), high monthly erosivity density values (greater than3 MJ ha − 1 h − 1) aid higher runoff prediction, and areas are exposed to flood risk and water scarcity. Estimation of the change in erosivity density will facilitate identification of the Boubo coastal watershed rainfall energy trends and possible climate change signals.

The shape, gradient, length, and location of slopes affect erosion. The slope length exponent in RUSLE2 is a function of land cover, soil biomass, and degree of soil consolidation, and varies daily. Owing to a lack of availability of data, we did not determine the effect of cover management on the slope length factor. The slope exponent in Eq. (9) was used without considering the effect of the cover management $\frac{c_{pr}}{c_{pt}}$.

RUSLE family models have been previously used to analyze soil erosion in Côte d'Ivoire (Alexis, 2015; Boyossoro et al., 2007; Coulibaly et al., 2007; Coulibaly Talnan et al., 2014; Koua et al., 2019; Mathieu, 1971; N'dri et al., 2017; Eblin et al., 2017; Vami Hermann et al., 2018). Our study shows that Boubo is highly vulnerable to soil erosion, similar to the vulnerability of most areas in Côte d'Ivoire. Côte d'Ivoire, a developing country, does not invest sufficient resources to effectively combat this phenomenon; however, the accelerated soil loss, which increased by 110% from 1990 to 2019 during June, should provide guidance to planners and decision-makers. Accelerated soil loss is an indicator of the impact of past climate change and changes in vegetation cover on soil erosion. RUSLE2 used with GIS should also include a method such as linear spectral unmixing to differentiate the mixing structure of land use units within pixels to improve the estimation of potential erosion areas. Estimation of the cover management in such an area via LSU may help improve the results of this method compared to those of other traditional methods that use NDVI. The spatial variation information in terms of precipitation and temperature should be integrated to improve the soil erodibility K factor estimation. This may help identify soil loss and sediment sources. Other studies have suggested an approach for the establishment forward soil erosion models (Batista et al., 2019). Recent studies have used a machine learning approach to predict soil erosion (Mosavi et al., 2020; Vu Dinh et al., 2021); however, the implementation of this approach in this area is challenging because of the lack of availability of data and time for data loading. This study identifies the northern part of the study area and the cities of Divo, Guitry, Lakota, and Diegonefla as being vulnerable to damage. Soil conservation planning should be coordinated across the Boubo watershed, and special measures should be implemented to prevent erosion. Soil is a non-renewable energy source that demonstrates many roles in the ecosystem. RUSLE-based GIS integrated with LSU can help prevent degradation of the landscape. Prevention of soil degradation may be an excellent strategy to improve soil productivity and human life. Prevention of accelerated erosion and runoff, rather than performing attempts to reduce runoff rates and sediment yield, would be adequate for water and sediment management. Water and sediment control practices should be implemented in the problematic location. Therefore, the Boubo coastal watershed should be investigated further by adopting methods such as analysis of the hydrologic frequency, opening of channel hydraulics, construction of sediment control structures, monitoring of hydrologic systems, and development of a deep maintenance program to prevent soil loss. Similarly, Lal (2009) has suggested that it is better to prevent soil erosion than to adopt practices for tackling eroded soil by improving the existing method. Soil conservation measures are absent in the Boubo watershed. However, Côte d'Ivoire is committed to creating an integrated national platform for sustainable land and water management. In Côte d'Ivoire, soil conservation measures are mainly focused on agroforestry, cultural rotation, and reforestation. Conservation planning should consider a vegetation restoration program and analyze its effects on soil erosion reduction in this area because vegetation management can help reduce erosion by up to 99% (Labrière et al., 2015). Vegetation restoration has been found to be an effective strategy to reduce soil erosion and to maintain soil productivity (Gu et al., 2018; Koua et al., 2019; Smith Dumont et al., 2014; Zhou et al., 2016).

Sediment yield increased from 1.09 t/ha/yr in 1990 to 2.54 t/ha/yr in 2019. Compared to the sediment yield information available on expansive African rivers, the years 1990 and 2019 present a low rate of sediment yield (Giresse, 2008). One improvement in RUSLE2 is the

consideration of runoff in the process of soil erosion and sedimentation (USDA-ARS, 2013). However, it was challenging to compare the results of this study to those of expansive rivers because of the lack of availability of data. Expansive rivers carry sand-type sediments and gravel-dominated bedloads, contradicting the concept of uniform sediment. However, smaller rivers mainly transport sand-type sediments. Therefore, the assumption that the sediment has a consistent grain size may be correct to a certain extent. Therefore, while studying an expansive river where the charge is dominated by gravel and where there is no uniformity in sediment size, the sediment loading models must be used with different considerations. Sediment yield is a direct threat to the lagoon in the Boubo coastal watershed because of siltation, and the ecological functions of soils are affected by erosion. We used SDR in Boubo for restoration planning and design purposes. However, this approach is subject to significant uncertainty and a general inability to relate sediment storage processes within the landscape and complex channels. Future studies in the Boubo watershed may be based on the use of geochemical tracers to identify sediment source and sink and to estimate sediment yield and soil erosion and deposition areas to establish watershed priorities. Our results on sediment transport were higher than those obtained using contemporary real-life case studies of soft computing techniques in the Kebir watershed (Amamra et al., 2018). This may be attributed to the different sizes of the watersheds and the methods used. As machine learning is a promising technique for sediment transport research, future research in the study area should be conducted to evaluate machine learning approaches to estimate soil erosion and sediment yield alongside extensive field data collection.

6. Advantages and limitations and future research

The RUSLE2 model demonstrates the advantage of incorporating many types of climatic data. The model considers seasonal variations in precipitation and temperature in soil erodibility, and can be used to perform calculations using temperature data rather than the data derived from existing graphs. The C factor that is used to describe the canopy's effect on erosion is a function of the top cover, antecedent soil moisture, soil roughness, and previous cultural practices. The effect of conservation practices on erosion rates has gained prominence as a function of contour lines, terraces, and drainage characteristics. The model can be used to estimate sediment yield and runoff in the rill area. RUSLE2 presents with several limitations: first, it is only applied to groundwater erosion because the energy source is rainfall. It has never been applied to linear erosion and has only been applied to average data covering a period of at least 20 years, neglecting specific interactions between factors (FAO-ITPS, 2015). RUSLE2 is not used while considering gully erosion; only interill and rill erosion are considered. Additionally, selection of a representative profile may be problematic, as erosion patterns change with slope steepness, length, soil type, and agricultural management; therefore, it is challenging to represent the profile in a GIS application. Hence, to improve the accuracy of the erosion hazard, identification and measurement of gullies in the watershed should be conducted to improve the accuracy of soil loss estimations for better planning and management in the future. This research demonstrates that remote sensing and GIS combined with RUSLE2 modeling provide a robust method for future studies related to soil erosion. The temporal variation in the K factor should be studied further in future studies. Alewell et al. (2019) discussed the limitations of the family model.

The study of the relationship between land use and soil erosion is the basis for revealing the source of sediment in rivers and for conducting river sediment prediction. Although existing studies have demonstrated the achievement of remarkable results, the following questions should be examined: first, various models have been established to study the relationship between land use and soil erosion. However, these models have been mostly limited to correlation analysis, and correlation analysis can be performed to only reflect trends between factors. The causal relationships remain unknown; therefore, these models present with several limitations. Second, most existing studies have focused on a single scale and multi-scale soil erosion research is limited, especially in the application of multi-scale soil erosion models. In the future, multi-scale research methods should be used to explore the soil erosion effects in this area at four different land use scales: the slope/field, small watershed, watershed, and regional scales. Multi-scale soil erosion studies may help identify different sources of sediments.

7. Conclusion

The new approach of integrating the RUSLE2 model with the LSU model has demonstrated the manner in which an improved RUSLE2 method can be used to better evaluate soil erosion and sediment yield in the Boubo coastal watershed. Previous studies have not examined soil erosion induced by water in this watershed using this approach. To maintain soil productivity and to protect the coastal ecosystem, it is vital to prevent topsoil removal by soil erosion and sedimentation.

The selected method will provide decision-makers and city planners with a better understanding of the evolution of erosion in the Boubo watershed. The study's findings reveal widespread accelerated soil erosion rates of low to moderate severity ranging from 40.89 to 94.99 t/km^2/year, as well as temperature change effects exerted on the K factor. The Boubo watershed is impacted by water erosion induced by human activities and climate change. The increased erosion rate from 1990 to 2019 is alarming, and all farmers and government authorities should undertake urgent steps for improved land management. Erosion is a combination of processes that vary in time and space based on environmental conditions and poor land management. Soil loss values computed via RUSLE2 integrated with LSU should be used as a reference rather than being considered absolute.

Limited studies on water erosion within the region have reduced the possibility of data comparison. However, this study has scientific and practical relevance to ecological restoration and water resource management.

On several areas of highly erodible cultivated land, water erosion can be economically reduced by only considering protective vegetation cover. Future research should be conducted to explore a machine-learning approach to estimate soil erosion and sediment yield, and to evaluate ecosystem management based on ecosystem services and sediment deposition in this area.

CRediT authorship contribution statement

Lenikpoho Karim Coulibaly: Conceptualization, Methodology, Validation, Formal analysis, Resources, Data curation, Writing - original draft, Writing - review & editing, Visualization. **Qingfeng Guan:** Supervision, Writing - review & editing, Resources, Visualization. **Tchimou Vincent Assoma:** Conceptualization, Writing - review & editing. **Fan Xin:** Resources. **Naga Coulibaly:** Writing - review & editing.

Declaration of Competing Interest

The authors declare that they have no known competing financial interests or personal relationships that could have appeared to influence the work reported in this paper.

References

Abdulkareem, J.H., Pradhan, B., Sulaiman, W.N.A., Jamil, N.R., 2019. Prediction of spatial soil loss impacted by long-term land-use/land-cover change in a tropical watershed. Geosci. Front. 10 (2), 389–403. https://doi.org/10.1016/j.gsf.2017.10.010.

Adams and Smith, 1986. Spectral mixture modeling: A new analysis of rock and soil types at the Viking Lander 1 Site. J. Geophys. Res. 91 (B8) https://doi.org/10.1029/JB091iB08p08098.

Alemaw, B.F., Majauale, M., Simalenga, T., 2013. Assessment of sedimentation impacts on small dams—a case of small reservoirs in the lotsane catchment. J. Water Resour. Prot. 05 (12), 1127–1131. https://doi.org/10.4236/jwarp.2013.512118.

Alewell, C., Borrelli, P., Meusburger, K., Panagos, P., 2019. Using the USLE: Chances, challenges and limitations of soil erosion modelling. Int. Soil Water Conserv. Res. 7 (3), 203–225. https://doi.org/10.1016/j.iswcr.2019.05.004.

Alexis, N.G.Y., 2015. Hydrologie et dynamique de l'état de surface des terres dans le sud-ouest de la Côte d'Ivoire : moteurs de dégradation impacts et moteurs de dégradation. University of Abobo-Adjame Abidjan.

Alizadeh, M.J., Jafari, N.E., Kalarestaghi, N., Chau, K.W., 2017. Toward multi-day-ahead forecasting of suspended sediment concentration using ensemble models. Environ. Sci. Pollut. Res. Int. 24 (36), 28017–28025. https://doi.org/10.1007/s11356-017-0405-4.

Almagro, A., Thomé, T.C., Colman, C.B., Pereira, R.B., Marcato, J.J., Rodrigues, D.B.B., Oliveira, P.T.S., 2019. Improving cover and management factor (C-factor) estimation using remote sensing approaches for tropical regions. Int. Soil Water Conserv. Res. 7 (4), 325–334. https://doi.org/10.1016/j.iswcr.2019.08.005.

Amamra, A., Khanchoul, K., Eslamian, S., Zobir, S.H., 2018. Suspended sediment estimation using regression and artificial neural network models: Kebir watershed, northeast of Algeria, North Africa. Int. J. Hydrol. Sci. Technol. 8 (4), 352. https://doi.org/10.1504/ijhst.2018.095526.

Arnold, J.G., Srinivasan, R., Muttiah, R.S., Williams, J.R., 1998. Large area hydrologic modeling and assessment Part I: Model development. J. Am. Water Resour. Assoc. 34 (1), 73–89.

Arnoldus, H.M.J., 1980. An Approximation of the Rainfall Factor in the Universal Soil Loss Equation. In: De Boodt, M., Gabriels, D. (Eds.), Assessment of Erosion. John Wiley and Sons, New York, pp. 127–132.

Asare-Kyei, D., Forkuor, G., Venus, V., 2015. Modeling flood hazard zones at the sub-district level with the rational model integrated with GIS and remote sensing approaches. Water 7 (12), 3531–3564. https://doi.org/10.3390/w7073531.

Asner, G.P., Heidebrecht, K.B., 2002. Spectral unmixing of vegetation, soil and dry carbon cover in arid regions: Comparing multispectral and hyperspectral observations. Int. J. Remote Sens. 23 (19), 3939–3958. https://doi.org/10.1080/01431160110115960.

Auerswald, K., Fiener, P., Martin, W., Elhaus, D., 2014. Use and misuse of the K factor equation in soil erosion modeling: An alternative equation for determining USLE nomograph soil erodibility values. Catena 118, 220–225. https://doi.org/10.1016/j.catena.2014.01.008.

Avenard J.M., Eldln M., Girard G., Sircoulon J., Touchebeuf P., Guillaumet J.L., Adjanohoun E. and Perraud A., 1971. Le milieu naturel de la côte d'ivoire. MÉMOIRES ORSTOM n 50. ORSTOM, (50), Paris.

Ayalew, D.A., Deumlich, D., Šarapatka, B., Doktor, D., 2020. Quantifying the Sensitivity of NDVI-Based C Factor Estimation and Potential Soil Erosion Prediction using Spaceborne Earth Observation Data. Remote Sens. 12 (7) https://doi.org/10.3390/rs12071136.

Bai, Z.G., Dent, D.L., Olsson, L., Schaepman, M.E., 2008. Global Assessment of Land Degradation and Improvement. 1. Identification by remote sensing, ISRIC –. World Soil Information, Wageningen.

Ballabio, C., Borrelli, P., Spinoni, J., Meusburger, K., Michaelides, S., Begueria, S., Klik, A., Petan, S., Janecek, M., Olsen, P., Aalto, J., Lakatos, M., Rymszewicz, A., Dumitrescu, A., Tadic, M.P., Diodato, N., Kostalova, J., Rousseva, S., Banasik, K., Alewell, C., Panagos, P., 2017. Mapping monthly rainfall erosivity in Europe. Sci. Total Environ. 579, 1298–1315. https://doi.org/10.1016/j.scitotenv.2016.11.123.

Baret, F., Weiss, M., Lacaze, R., Camacho, F., Makhmara, H., Pacholcyzk, P., Smets, B., 2013. GEOV1: LAI and FAPAR essential climate variables and FCOVER global time series capitalizing over existing products. Part1: Principles of development and production. Remote Sens. Environ. 137, 299–309. https://doi.org/10.1016/j.rse.2012.12.027.

Baskan, O., Dengiz, O., 2008. Comparison of Traditional and Geostatistical Methods to Estimate Soil Erodibility Factor. Arid Land Res. Manage. 22 (1), 29–45. https://doi.org/10.1080/15324980701784241.

Batista, P.V.G., Davies, J., Silva, M.L.N., Quinton, J.N., 2019. On the evaluation of soil erosion models: Are we doing enough? Earth-Sci. Rev. 197 https://doi.org/10.1016/j.earscirev.2019.102898.

Benaud, P., Anderson, K., Evans, M., Farrow, L., Glendell, M., James, M.R., Quine, T.A., Quinton, J.N., Rawlins, B., Jane Rickson, R., Brazier, R.E., 2020. National-scale geodata describe widespread accelerated soil erosion. Geoderma 371. https://doi.org/10.1016/j.geoderma.2020.114378.

Benavidez, R., Jackson, B., Maxwell, D., Norton, K., 2018. A review of the (Revised) Universal Soil Loss Equation ((R)USLE): with a view to increasing its global applicability and improving soil loss estimates. Hydrol. Earth Syst. Sci. 22 (11), 6059–6086. https://doi.org/10.5194/hess-22-6059-2018.

Borrelli, P., Alewell, C., Alvarez, P., Anache, J.A.A., Baartman, J., Ballabio, C., Bezak, N., Biddoccu, M., Cerda, A., Chalise, D., Chen, S., Chen, W., De Girolamo, A.M., Gessesse, G.D., Deumlich, D., Diodato, N., Efthimiou, N., Erpul, G., Fiener, P., Freppaz, M., Gentile, F., Gericke, A., Haregeweyn, N., Hu, B., Jeanneau, A., Kaffas, K., Kiani-Harchegani, M., Villuendas, I.L., Li, C., Lombardo, L., Lopez-Vicente, M., Lucas-Borja, M.E., Marker, M., Matthews, F., Miao, C., Mikos, M., Modugno, S., Moller, M., Naipal, V., Nearing, M., Owusu, S., Panday, D., Patault, E., Patriche, C.V., Poggio, L., Portes, R., Quijano, L., Rahdari, M.R., Renima, M., Ricci, G.F., Rodrigo-Comino, J., Saia, S., Samani, A.N., Schillaci, C., Syrris, V., Kim, H.S., Spinola, D.N., Oliveira, P.T., Teng, H., Thapa, R., Vantas, K., Vieira, D., Yang, J.E., Yin, S., Zema, D.A., Zhao, G., Panagos, P., 2021. Soil erosion modelling: A global review and statistical analysis. Sci. Total Environ. 780, 146494 https://doi.org/10.1016/j.scitotenv.2021.146494.

Borrelli, P., Märker, M., Schütt, B., 2015. Modelling Post-Tree-Harvesting Soil Erosion and Sediment Deposition Potential in the Turano River Basin (Italian Central Apennine). Land Degrad. Dev. 26 (4), 356–366. https://doi.org/10.1002/ldr.2214.

Boyossoro, Koffi, Bachir, Biémi and Traoré, 2007. Insécurité climatique et géorisques en Côte d'Ivoire : étude du risque d'érosion hydrique des sols dans la région semi-montagneuse de Man (Ouest de la Côte d'Ivoire). 29-37. https://www.doi.org/10.1684/sec.2007.0064.

Su, C., Fu, B., Wei, Yongping, Yihe Lü, G., Liu, Daolong Wang, Mao, K., Feng, X., 2011. Ecosystem management based on ecosystem services and human activities: a case study in the Yanhe watershed. Sustain. Sci. 7 (1), 17–32. https://doi.org/10.1007/s11625-011-0145-1.

Chai, T., Draxler, R.R., 2014. Root mean square error (RMSE) or mean absolute error (MAE)? – Arguments against avoiding RMSE in the literature. Geosci. Model Dev. 7 (3), 1247–1250. https://doi.org/10.5194/gmd-7-1247-2014.

Chen, X.-Y., Chau, K.-W., 2019. Uncertainty Analysis on Hybrid Double Feedforward Neural Network Model for Sediment Load Estimation with LUBE Method. Water Resour. Manage. 33 (10), 3563–3577. https://doi.org/10.1007/s11269-019-02318-4.

Cheng, Z., Lu, D., Li, G., Huang, J., Sinha, N., Zhi, J., Li, S., 2018. A random forest-based approach to map soil erosion risk distribution in hickory plantations in western Zhejiang province, China. Remote Sens. 10 (12) https://doi.org/10.3390/rs10121899.

Colman, C.B., Garcia, K.M.P., Pereira, R.B., Shinma, E.A., Lima, F.E., Gomes, A.O., Oliveira, P.T.S., 2018. Different approaches to estimate the sediment yield in a tropical watershed. Rbrh 23. https://doi.org/10.1590/2318-0331.231820170178.

Coulibaly, N., Goula, B.T.A., Coulibaly, L., I. S., 2007. Modélisation Spatio-Temporelles De L'érosion Hydrique À Partir L'usle En Zone De Savane Tropicale Humide : Cas Du Bassin Versant Du Bâoulé (Côte D'ivoire). Eur. J. Sci. Res. 16 (2), 213–221.

Coulibaly Talnan, J.H., Naga, Coulibaly, Donald, Koffi, Mathurin, Camara, Issiaka, S., 2014. Cartographie des zones à l'origine de l'ensablement des canaux du bassin versant du Gourou (Abidjan – Côte d'Ivoire). Int. J. Innovation Appl. Stud. 6 (3), 642–653.

Cristiano, E., ten Veldhuis, M.-C., van de Giesen, N., 2017. Spatial and temporal variability of rainfall and their effects on hydrological response in urban areas – a review. Hydrol. Earth Syst. Sci. 21 (7), 3859–3878. https://doi.org/10.5194/hess-21-3859-2017.

Dabney, Yoder and Vieira, 2015. Erosion Modeling in 2D with the Revised Universal Soil Loss Equation Version 2: A Tool for Conservation Planning. In: Tom Mueller and G.F. Sassenrath (Editors), GIS Applications in Agriculture Conservation Planning, Boca Raton, pp. 69-83.

Dabney, S.M., Yoder, D.C., Vieira, D.A.N., Bingner, R.L., 2011. Enhancing RUSLE to include runoff-driven phenomena. Hydrol. Process. 25 (9), 1373–1390. https://doi.org/10.1002/hyp.7897.

De Asis, A.M., Omasa, K., 2007. Estimation of vegetation parameter for modeling soil erosion using linear Spectral Mixture Analysis of Landsat ETM data. J. Photogramm. Remote Sens. 62 (4), 309–324. https://doi.org/10.1016/j.isprsjprs.2007.05.013.

De Asis, A.M., Omasa, K., Oki, K., Shimizu, Y., 2008. Accuracy and applicability of linear spectral unmixing in delineating potential erosion areas in tropical watersheds. Int. J. Remote Sens. 29 (14), 4151–4171. https://doi.org/10.1080/01431160701874579.

De Jong, S.M., 1994. Derivation of vegetative variables from a landsat tm image for modelling soil erosion. Earth Surf. Process. Landf. 19 (2), 165–178. https://doi.org/10.1002/esp.3290190207.

Desmet and Govers, 1996. A GIS Procedure for Automatically Calculating the USLE LS Factor on Topographically Complex Landscape Units. J. Soil Water Conserv. 51, 427–433.

Dutta, S., 2016. Soil erosion, sediment yield and sedimentation of reservoir: a review. Model Earth Syst. Environ. 2 (3) https://doi.org/10.1007/s40808-016-0182-y.

Ebrahimzadeh, S., Motagh, M., Mahboub, V., Mirdar, Harijani F., 2018. An improved RUSLE/SDR model for the evaluation of soil erosion. Environ. Earth Sci. 77 (12) https://doi.org/10.1007/s12665-018-7635-8.

Elmore, A.J., Mustard, J.F., Manning, S.J., Lobell, D.B., 2000. Quantifying Vegetation Change in Semiarid Environments. Remote Sens. Environ. 73 (1), 87–102. https://doi.org/10.1016/s0034-4257(00)00100-0.

FAO-ITPS, 2015. Status of the World's Soil Resources, Rome, Italy.

FAO, 2015. Status of the World's Main Report Soil Resources.

Farhan, Y., Nawaiseh, S., 2015. Spatial assessment of soil erosion risk using RUSLE and GIS techniques. Environ. Earth Sci. 74 (6), 4649–4669. https://doi.org/10.1007/s12665-015-4430-7.

Ferreira, V., Panagopoulos, T., 2014. Seasonality of soil erosion under mediterranean conditions at the Alqueva Dam watershed. Environ. Manage. 54 (1), 67–83. https://doi.org/10.1007/s00267-014-0281-3.

Ferro, V., 1997. Further remarks on a distributed approach to sediment delivery. Hydrol. Sci. 42 (5), 633–647.

Ferro, V., Minacapilli, M., 1995. Sediment delivery processes at basin scale. Hydrol. Sci. 40 (6), 703–717.

Ferro, V., Porto, P., Tusa, G., 1998. Testing a distributed approach for modelling sediment delivery. Hydrol. Sci. 43 (3), 425–442.

Foster and Wischmeier, 1974. Evaluating Irregular Slopes for Soil Loss Prediction. Trans. ASAE 17 (2), 0305–0309. https://doi.org/10.13031/2013.36846.

Foster, G.R., S G. A. Weesies, D. K. McCool, D. C. Yoder and Renard K.G., 1999. Revised Universal Soil Loss Equation user's manual.

Fu, B., Liu, Y., Lü, Y., He, C., Zeng, Y., Wu, B., 2011. Assessing the soil erosion control service of ecosystems change in the Loess Plateau of China. Ecol. Complex. 8 (4), 284–293. https://doi.org/10.1016/j.ecocom.2011.07.003.

García-Haro, F.J., Camacho, F., Martínez, B., Campos-Taberner, M., Fuster, B., Sánchez-Zapero, J., Gilabert, M.A., 2019. Climate data records of vegetation variables from geostationary SEVIRI/MSG data: products. Algorithms and Applications. Remote Sens. 11 (18) https://doi.org/10.3390/rs11182103.

Garcia-Ruiz, José M., Santiago, B., Noemí, L.R., Estela, N.R., Artemi, C., 2016. Ongoing and emerging questions in water erosion studies. Land Degrad. Dev. 28 (1), 5–21. https://doi.org/10.1002/ldr.2641.

Gertner, G., Wang, G., Fang, S., Anderson, A.B., 2002. Mapping and uncertainty of predictions based on multiple primary variables from joint co-simulation with Landsat TM image and polynomial regression. Remote Sens. Environ. 83 (3), 498–510. https://doi.org/10.1016/s0034-4257(02)00066-4.

Ghosal, K., Das Bhattacharya, S., 2020. A Review of RUSLE Model. J. Indian Soc. Remote Sens. 48 (4), 689–707. https://doi.org/10.1007/s12524-019-01097-0.

Giresse, P., 2008. Present fluxes of suspended and dissolved matter in rivers, tropical and sub-tropical west africa - marine and continental changes during the late quaternary. Developments in Quaternary Sciences 19–28. https://doi.org/10.1016/s1571-0866(08)80006-1.

Golian, M., Katibeh, H., Singh, V.P., Ostad-Ali-Askari, K., Rostami, H.T., 2020. Prediction of tunnelling impact on flow rates of adjacent extraction water wells. Q. J. Eng. Geol. Hydrogeol. 53 (2), 236–251. https://doi.org/10.1144/qjegh2019-055.

Grazhdani, S., Shumka, S., 2007. An approach to mapping soil erosion by water with application to Albania. Desalination 213 (1–3), 263–272. https://doi.org/10.1016/j.desal.2006.03.612.

Gu, Z., Xie, Y., Gao, Y., Ren, X., Cheng, C., Wang, S., 2018. Quantitative assessment of soil productivity and predicted impacts of water erosion in the black soil region of northeastern China. Sci. Total Environ. 637–638, 706–716. https://doi.org/10.1016/j.scitotenv.2018.05.061.

Hajigholizadeh, M., Melesse, A.M., Fuentes, H.R., 2018. Erosion and Sediment Transport Modelling in Shallow Waters: A Review on Approaches, Models and Applications. Int. J. Environ. Res. Public Health 15 (3). https://doi.org/10.3390/ijerph15030518.

Hamontree, C., Anh Nguyen, K., Chen, W., 2018. Estimating sediment delivery ratio by stream slope and relief ratio. MATEC Web of Conferences 192. https://doi.org/10.1051/matecconf/201819202040.

Her, Y., 2011. HYSTAR: Hydrology and Sediment Transport Simulation using Time-Area Method. Virginia Polytechnic Institute and State University.

Hrabalíková, M., Janeček, M., 2017. Comparison of different approaches to LS factor calculations based on a measured soil loss under simulated rainfall. Soil and Water Research 12 (2), 69–77. https://doi.org/10.17221/222/2015-swr.

Huang, Chenlu, Yang, Qinke, Cao, Xiayu, Li, Yuru, 2020. Assessment of the Soil Erosion Response to Land Use and Slope in the Loess Plateau—A Case Study of Jiuyuangou. Water 12 (2), 529. https://doi.org/10.3390/w12020529.

IUCN, 2016. Opportunities for Restoring Degraded Forests and Landscapes in Ivory Coast.

Jain, M.K., Das, D., 2009. Estimation of sediment yield and areas of soil erosion and deposition for watershed prioritization using GIS and remote sensing. Water Resour. Manage. 24 (10), 2091–2112. https://doi.org/10.1007/s11269-009-9540-0.

Jain, M.K., Mishra, S.K., Shah, R.B., 2009. Identification of sediment source and sink areas in a Himalayan watershed using GIS and remote sensing. Land Degrad. Dev. 20 (6), 623–639. https://doi.org/10.1002/ldr.952.

Jebari, S., Berndtsson, R., Olsson, J., Bahri, A., 2012. Soil erosion estimation based on rainfall disaggregation. J. Hydrol. 436–437, 102–110. https://doi.org/10.1016/j.jhydrol.2012.03.001.

Jianxiang, Z., Zhang, D., Liu, W., Hu, A., Sun, B., Zhang, Y., 2019. Progress in research on land use and soil erosion in the Loess Plateau of China, IOP Conference Series: Earth and Environmental Science. https://www.doi.org/10.1088/1755-1315/242/5/052021.

Jimenez-Munoz, J.C., Sobrino, J.A., Plaza, A., Guanter, L., Moreno, J., Martinez, P., 2009. Comparison Between Fractional Vegetation Cover Retrievals from Vegetation Indices and Spectral Mixture Analysis: Case Study of PROBA/CHRIS Data Over an Agricultural Area. Sensors (Basel) 9 (2), 768–793. https://doi.org/10.3390/s90200768.

Karydas, C., Petriolis, M., Manakos, I., 2013. Evaluating Alternative Methods of Soil Erodibility Mapping in the Mediterranean Island of Crete. Agriculture 3 (3), 362–380. https://doi.org/10.3390/agriculture3030362.

Karydas, C.G., Panagos, P., Gitas, I.Z., 2012. A classification of water erosion models according to their geospatial characteristics. Int. J. Digit. Earth 7 (3), 229–250. https://doi.org/10.1080/17538947.2012.671380.

Karydas, C.G., Sekuloska, T., Silleos, G.N., 2009. Quantification and site-specification of the support practice factor when mapping soil erosion risk associated with olive plantations in the Mediterranean island of Crete. Environ. Monit. Assess. 149 (1–4), 19–28. https://doi.org/10.1007/s10661-008-0179-8.

Kerdiles, H., Grondona, M.O., 1995. NOAA-AVHRR NDVI decomposition and subpixel classification using linear mixing in the Argentinean Pampa. Int. J. Remote Sens. 16 (7), 1303–1325. https://doi.org/10.1080/01431169508954478.

Kidane, M., Bezie, A., Kesete, N., Tolessa, T., 2019. The impact of land use and land cover (LULC) dynamics on soil erosion and sediment yield in Ethiopia. Heliyon 5 (12). https://doi.org/10.1016/j.heliyon.2019.e02981.

Kijowska-Strugała, M., Bucała-Hrabia, A., Demczuk, P., 2018. Long-term impact of land use changes on soil erosion in an agricultural catchment (in the Western Polish Carpathians). Land Degrad. Dev. 29 (6), 1871–1884. https://doi.org/10.1002/ldr.v29.610.1002/ldr.2936.

Kinnell,, 2010. Event soil loss, runoff and the Universal Soil Loss Equation family of models: A review. J. Hydrol. 385 (1–4), 384–397. https://doi.org/10.1016/j.jhydrol.2010.01.024.

Kinnell,, 2019. A Review of the Science and Logic Associated with Approach Used in the Universal Soil Loss Equation Family of Models. Soil Syst. 3 (4) https://doi.org/10.3390/soilsystems3040062.

Kothyari, U.C., Jain, M.K., Ranga Raju, K.G., 2002. Estimation of temporal variation of sediment yield using GIS / Estimation de la variation temporelle de l'exportation sédimentaire grâce à un SIG. Hydrol. Sci. J. 47 (5), 693–706. https://doi.org/10.1080/02626660209492974.

Koua, J.-J.T., Anoh, A.K., Soro, D.T., Kouame, J.K., Jourda, R.J.P., 2019. Evaluation of Agricultural Practices Scenarios for Reducing Erosion in Buyo Lake Catchment (Sassandra; Côte d'Ivoire) by Use of GIS. J. Geosci. Environ. Prot. 07 (07), 154–171. https://doi.org/10.4236/gep.2019.77011.

Kouadio, Z.A., 2011. Dynamique de l'occupation du sol et comportement hydrologique: cas des bassins versants côtiers de l'Agneby et du Boubo (Cote D'Ivoire). Nangui Abrogoua University, Abidjan.

Labrière, N., Locatelli, B., Laumonier, Y., Freycon, V., Bernoux, M., 2015. Soil erosion in the humid tropics: A systematic quantitative review. Agric., Ecosyst. Environ. 203 https://doi.org/10.1016/j.agee.2015.01.027.

Lal, R., 2001. Soil degradation by erosion. Land Degrad. Dev. 12 (6), 519–539. https://doi.org/10.1002/ldr.472.

Lal, R., 2009. Soil erosion and sediment transport research in tropical Africa. Hydrol. Sci. J. 30 (2), 239–256. https://doi.org/10.1080/02626668509490987.

Lal R., 2014. Soil conservation and ecosystem services. Int.Soil Water Conserv. Res., 2(3): 36-47. https://www.doi.org/10.1016/s2095-6339(15)30021-6.

Lal R., 2015. Restoring Soil Quality to Mitigate Soil Degradation. Sustainability, 7(5): 5875-5895. https://www.doi.org/10.3390/su7055875.

Lanckriet, S., Asfaha, T., Frankl, A., Zenebe, A. Nyssen, J., 2016. Sediment in Alluvial and Lacustrine Debris Fans as an Indicator for Land Degradation Around Lake Ashenge (Ethiopia). Land Degrad. Dev., 27(2): 258-269. https://www.doi.org/10.1002/ldr.2424.

Latocha, A., Szymanowski, M., Jeziorska, J., Stec, M., Roszczewska, M., 2016. Effects of land abandonment and climate change on soil erosion—An example from depopulated agricultural lands in the Sudetes Mts. SW Poland. Catena 145, 128–141. https://doi.org/10.1016/j.catena.2016.05.027.

Lewis L.A., 2013. Simulation of Soil Erosion and Sedimentation in Small River Basins. Phys. Geogr., 1(2): 172-176. https://www.doi.org/10.1080/02723646.1980.10642198.

Li, X., Qiu, J., Shang, Q., Li, F., 2016. Simulation of Reservoir Sediment Flushing of the Three Gorges Reservoir Using an Artificial Neural Network. Applied Sciences, 6(5). https://www.doi.org/10.3390/app6050148.

Li, Z., Fang, H., 2016. Impacts of climate change on water erosion: A review. Earth-Sci. Rev., 163: 94-117. https://www.doi.org/10.1016/j.earscirev.2016.10.004.

Lim, K.J., Sagong, M., Engel, B.A., Tang, Z., Choi, J., Kim, K.-S., 2005. GIS-based sediment assessment tool. Catena, 64(1): 61-80. https://www.doi.org/10.1016/j.catena.2005.06.013.

Liu, L., Su, R., Ostad-Ali-Askar, K., 2018. Water resources and climate change. Journal of Water and Climate Change, 9(2): 239-239. https://doi.org/10.2166/wcc.2018.999.

Lu, D., Li, G., Valladares, G.S., Batistella, M., 2004. Mapping soil erosion risk in Rondônia, Brazilian Amazonia: using RUSLE, remote sensing and GIS. Land Degrad. Dev., 15(5): 499-512. https://www.doi.org/10.1002/ldr.634.

M. N., S. C., S O., G. M. and C. Z., Simulation of field-measured soil loss in Mediterranean hilly areas (Chianti, Italy) with RUSLE Catena 145 2016 246 256 https://www.doi.org/10.1016/j.catena.2016.06.018.

M.E.D.D., 2019. Résumé d'information de la Côte d'Ivoire sur la prise en compte des garanties de la REDD+ sur la période 2015–2018. Ministère de l'Environnement et du Développement Durable, Abidjan.

Ma, J.W., Xue, Y., Ma, C.F., Wang, Z.G., 2010. A data fusion approach for soil erosion monitoring in the Upper Yangtze River Basin of China based on Universal Soil Loss Equation (USLE) model. Int. J. Remote Sens. 24 (23), 4777–4789. https://doi.org/10.1080/0143116021000056028.

Maeda, E.E., Formaggio, A.R., Shimabukuro, Y.E., 2013. Impacts of Land Use and Land Cover Changes on Sediment Yield in a Brazilian Amazon Drainage Basin. GiSci Remote Sens. 45 (4), 443–453. https://doi.org/10.2747/1548-1603.45.4.443.

Maner, 1958. Factors Affecting Sediment Delivery Rates in the Red Hills Physiographic Area. https://doi.org/10.1029/TR039i004p00669.

Mathieu, 1971. Erosion et transport sur un bassin versant forestier tropical (bassin de l'amitioro, sud de la côte d'ivoire). Cahl. ORSTOM, , sér. Géol., III, 2, : 115-144.

McCool, Foster and Yoder, 2004. The Revised Universal Soil Loss Equation, version 2. 13th International Soil Conservation Organisation Conference – Brisbane.

Merritt, W.S., Letcher, R.A., Jakeman, A.J., 2003. A review of erosion and sediment transport models. Environ. Model. Software, 18(8-9): 761-799. https://www.doi.org/10.1016/s1364-8152(03)00078-1.

Meusburger, K., Bänninger, D., Alewell, C., 2010a. Estimating vegetation parameter for soil erosion assessment in an alpine catchment by means of QuickBird imagery. Int J Appl Earth Obs. 12 (3), 201–207. https://doi.org/10.1016/j.jag.2010.02.009.

Meusburger, K., Konz, N., Schaub, M., Alewell, C., 2010b. Soil erosion modelled with USLE and PESERA using QuickBird derived vegetation parameters in an alpine catchment. Int J Appl Earth Obs. 12 (3), 208–215. https://doi.org/10.1016/j.jag.2010.02.004.

Milliman, J.D., Farnsworth, K.L., 2011. River Discharge to the Coastal Ocean- A Global Synthesis. Cambridge University Press. https://doi.org/10.1017/CBO9780511781247.

Mondal, A., Khare, D., Kundu, S., 2016. A comparative study of soil erosion modelling by MMF. USLE and RUSLE. Geocarto Int. 33 (1), 89–103. https://doi.org/10.1080/10106049.2016.1232313.

Montandon, L., Small, E., 2008. The impact of soil reflectance on the quantification of the green vegetation fraction from NDVI. Remote Sens. Environ. 112 (4), 1835–1845. https://doi.org/10.1016/j.rse.2007.09.007.
Mosavi, A., Sajedi-Hosseini, F., Choubin, B., Taromideh, F., Rahi, G., Dineva, A., 2020. Susceptibility Mapping of Soil Water Erosion Using Machine Learning Models. Water 12 (7). https://doi.org/10.3390/w12071995.
Myneni, R.B., Maggion, S., Iaquinta, J., Privette, J.L., Gobron, N., Pinty, B., Williams, D. L., 1995. Optical remote sensing of vegetation: Modeling, caveats, and algorithms. Remote Sens. Environ. 51 (1), 169–188. https://doi.org/10.1016/0034-4257(94)00073-v.
N'dri B.É., Niamke K.H., Koudou A. and N'go Y.A., 2017. Cartographie des formes d'érosion hydrique dans la commune urbaine d'attécoubé (abidjan, côte d'ivoire). International Journal of Innovation and Applied Studies, Vol. 19 No. 4: pp. 960-968.
Oldeman L.R., 1992. Global Extent of Soil Degradation, ISRIC Bi-Annual report.
Olorunfemi, I.E., Komolafe, A.A., Fasinmirin, J.T., Olufayo, A.A., Akande, S.O., 2020. A GIS-based assessment of the potential soil erosion and flood hazard zones in Ekiti State, Southwestern Nigeria using integrated RUSLE and HAND models. Catena 194. https://doi.org/10.1016/j.catena.2020.104725.
ONU-REDD+, 2017. Données forestières de base pour la redd+ en côte d'ivoire: Cartographie de la dynamique forestière de 1986 à 2015.
Ostad-Ali-Askari, K., Ghorbanizadeh, Kharazi H., Shayannejad, M., Zareian, M.J., 2019. Effect of management strategies on reducing negative impacts of climate change on water resources of the Isfahan-Borkhar aquifer using MODFLOW. River Res. Appl. 35 (6), 611–631. https://doi.org/10.1002/rra.3463.
Ostad-Ali-Askari, Kaveh, Ghorbanizadeh Kharazi, Hossein, Shayannejad, Mohammad, Zareian, Mohammad Javad, 2020. Effect of Climate Change on Precipitation Patterns in an Arid Region Using GCM Models: Case Study of Isfahan-Borkhar Plain. Nat. Hazards Rev. 21 (2), 04020006. https://doi.org/10.1061/(ASCE)NH.1527-6996.0000367.
Ostad-Ali-Askari K., Shayannejad, M., 2021. Quantity and quality modelling of groundwater to manage water resources in Isfahan-Borkhar Aquifer. Environ. Dev. Sustainability. https://doi.org/10.1007/s10668-021-01323-1.
Ostad-Ali-Askari, K., Shayannejad, M., Ghorbanizadeh-Kharazi, H., 2016. Artificial neural network for modeling nitrate pollution of groundwater in marginal area of Zayandeh-rood River, Isfahan. Iran. KSCE J. Civ. Eng. 21 (1), 134–140. https://doi.org/10.1007/s12205-016-0572-8.
Pan, J., Wen, Y., 2013. Estimation of soil erosion using RUSLE in Caijiamiao watershed. China. Nat. Hazards 71 (3), 2187–2205. https://doi.org/10.1007/s11069-013-1006-2.
Panagos, P., Ballabio, C., Borrelli, P., Meusburger, K., 2016. Spatio-temporal analysis of rainfall erosivity and erosivity density in Greece. Catena 137, 161–172. https://doi.org/10.1016/j.catena.2015.09.015.
Panagos, P., Borrelli, P., Meusburger, K., Alewell, C., Lugato, E., Montanarella, L., 2015. Estimating the soil erosion cover-management factor at the European scale. Land Use Policy 48, 38–50. https://doi.org/10.1016/j.landusepol.2015.05.021.
Panagos, P., Karydas, C.G., Gitas, I.Z., Montanarella, L., 2012. Monthly soil erosion monitoring based on remotely sensed biophysical parameters: a case study in Strymonas river basin towards a functional pan-European service. Int. J. Digit. Earth 5 (6), 461–487. https://doi.org/10.1080/17538947.2011.587897.
Panagos, P., Katsoyiannis, A., 2019. Soil erosion modelling: The new challenges as the result of policy developments in Europe. Environ. Res. 172, 470–474. https://doi.org/10.1016/j.envres.2019.02.043.
Papaiordanidis, S., Gitas, I.Z., Katagis, T., 2020. Soil erosion prediction using the Revised Universal Soil Loss Equation (RUSLE) in Google Earth Engine (GEE) cloud-based platform. Dokuchaev Soil Bulletin 100, 36–52. https://doi.org/10.19047/0136-1694-2019-100-36-52.
Papanicolaou, A.N., Elhakeem, M., Krallis, G., Prakash, S., Edinger, J., 2008. Sediment Transport Modeling Review—Current and Future Developments. J. Hydraul. Eng. 134 (1), 1–14. https://doi.org/10.1061/(ASCE)0733-9429(2008)134:1(1).
Patil, R.J., 2018. Spatial Techniques for Soil Erosion Estimation Remote Sensing and GIS Approach. https://doi.org/10.1007/978-3-319-74286-1.
Mather, Paul M., Koch, M., 2011. Computer Processing of Remotely Sensed Images An Introduction. Fourth Edition. https://doi.org/10.1002/9780470666517.
Pham, T.G., Degener, J., Kappas, M., 2018. Integrated universal soil loss equation (USLE) and Geographical Information System (GIS) for soil erosion estimation in A Sap basin: Central Vietnam. Int. Soil Water Conserv. Res. 6 (2), 99–110. https://doi.org/10.1016/j.iswcr.2018.01.001.
Phinzi, K., Ngetar, N.S., 2019. The assessment of water-borne erosion at catchment level using GIS-based RUSLE and remote sensing: A review. Int. Soil Water Conserv. Res. 7 (1), 27–46. https://doi.org/10.1016/j.iswcr.2018.12.002.
Pirnazar, M., Hasheminasab, H., Karimi, A.Z., 2018. The evaluation of the usage of the fuzzy algorithms in increasing the accuracy of the extracted land use maps. Int. J. Global Environmental Issues 17 (4), 307. https://doi.org/10.1504/IJGENVI.2018.095063.
Qiang, F., Wenwu, Z., 2014. The study on cover management factor in USLE and RUSLE: a review. ACTA ECOLOGICA SINICA, 34(16): 4461- 4472. https://www.doi.org/10.5846 /stxb201306151710.
REDD+, 2018. Readiness Package (R-Package) pour la Réduction des Emissions issues de la Déforestation et de la dégradation forestière en Côte d'Ivoire.
Reisenbüchler, M., Bui, M.D., Rutschmann, P., 2021. Reservoir Sediment Management Using Artificial Neural Networks: A Case Study of the Lower Section of the Alpine Saalach River. Water 13 (6). https://doi.org/10.3390/w13060818.
Renard, Foster, Weesies, McCool and Yoder, 1997. Predicting soil erosion by water: a guide to conservation planning with the revised universal soil loss equation (RUSLE). U.S. Department of Agriculture, Agriculture Handbook No. 703.
Renfro, 1975. Use of erosion equations and sediment delivery ratios for predicting sediment yield, in present and prospective technology for predicting sediment yield and sources. Washington: USDA: 33-45.
Roberts, D.A., Smith, M.O., Adams, J.B., 1993. Green vegetation, nonphotosynthetic vegetation, and soils in AVIRIS data. Remote Sens. Environ. 44 (2–3), 255–269. https://doi.org/10.1016/0034-4257(93)90020-x.
Roose, 1975. Application a l'equation de prevision de l'erosion de wishmeir et smith en afrique de l'ouest.
Roose, 1977. erosion et ruisselement en afrique de l'ouest.
Roose, 1983. Runoff and erosion before and after clearing depending on the type of crop in western Africa.
Roose, 1996. Land husbandry: Components and strategy.
Eblin, S.G., Yao, A.B., Anoh, A.K., Soro, N., 2017. Mapping of multifactorial vulnerability to soil erosion risks in the region of Adiaké, south-east coastal of Côte d'Ivoire. Rev. Ivoir. Sci. Technol. 30, 197–216.
Schmidt, S., Alewell, C., Meusburger, K., 2018. Mapping spatio-temporal dynamics of the cover and management factor (C-factor) for grasslands in Switzerland. Remote Sens. Environ. 211, 89–104. https://doi.org/10.1016/j.rse.2018.04.008.
Schmidt, S., Alewell, C., Meusburger, K., 2019. Monthly RUSLE soil erosion risk of Swiss grasslands. J MAPS. 15 (2), 247–256. https://doi.org/10.1080/17445647.2019.1585980.
Schmidt, S., Alewell, C., Panagos, P., Meusburger, K., 2016. Regionalization of monthly rainfall erosivity patterns in Switzerland. Hydrol. Earth Syst. Sci. 20 (10), 4359–4373. https://doi.org/10.5194/hess-20-4359-2016.
Sébastien, O.K., Denis, Y.-K., Salla, M., Félix, T.Z., 2013. Water Quality Assessment of the Coastal Tropical River'Sboubo (Côte d'Ivoire): Physico-Chemical and Biological Aspects. Journal of Environment Pollution and Human Health 1 (2), 9–15. https://doi.org/10.12691/jephh-1-2-1.
Sharafati, A., Haji Seyed Asadollah, S.B., Motta, D., Yaseen, Z.M., 2020. Application of newly developed ensemble machine learning models for daily suspended sediment load prediction and related uncertainty analysis. Hydrol. Sci. J. 65 (12), 2022–2042. https://doi.org/10.1080/02626667.2020.1786571.
Shelestov, A., Lavreniuk, M., Kussul, N., Novikov, A., Skakun, S., 2017. Exploring Google Earth Engine Platform for Big Data Processing: Classification of Multi-Temporal Satellite Imagery for Crop Mapping. Frontiers. Earth Sci. 5 https://doi.org/10.3389/feart.2017.00017.
Small, C., 2003. High spatial resolution spectral mixture analysis of urban reflectance. Remote Sens. Environ. 88 (1–2), 170–186. https://doi.org/10.1016/j.rse.2003.04.008.
Smith, Ustin S.L., Adams, J.B., Gillespie, A.R., 1990. Vegetation in deserts: I. A regional measure of abundance from multispectral images. Remote Sens. Environ. 31 (1), 1–26. https://doi.org/10.1016/0034-4257(90)90074-v.
Smith, Dumont E., Gnahoua, G.M., Ohouo, L., Sinclair, F.L., Vaast, P., 2014. Farmers in Côte d'Ivoire value integrating tree diversity in cocoa for the provision of ecosystem services. Agrofor. Syst. 88 (6), 1047–1066. https://doi.org/10.1007/s10457-014-9679-4.
Song, W., Mu, X., Ruan, G., Gao, Z., Li, L., Yan, G., 2017. Estimating fractional vegetation cover and the vegetation index of bare soil and highly dense vegetation with a physically based method. Int J Appl Earth Obs. 58, 168–176. https://doi.org/10.1016/j.jag.2017.01.015.
Spaeth, K.E., Pierson, F.B., Weltz, M.A., Blackburn, W.H., 2003. Evaluation of USLE and RUSLE estimated soil loss on rangeland. J. Range Manag. 56 (3) https://doi.org/10.2458/azu_jrm_v56i3_spaeth.
Sun, G., McNulty, S.G., 1998. Modeling soil erosion and transport on forest landscape, Proceedings of 29th International Conference on Erosion Control Association: 187–198. Reno, Nevada, pp. 187–198.
Sun, Z., Xu, R., Du, W., Wang, L., Lu, D., 2019. High-Resolution Urban Land Mapping in China from Sentinel 1A/2 Imagery Based on Google Earth Engine. Remote Sens. 11 (7) https://doi.org/10.3390/rs11070752.
Syrbe, R.-U., Schorcht, M., Grunewald, K., Meinel, G., 2018. Indicators for a nationwide monitoring of ecosystem services in Germany exemplified by the mitigation of soil erosion by water. Ecol. Indicators 94, 46–54. https://doi.org/10.1016/j.ecolind.2017.05.035.
Tadele, H., Mekuriaw, A., Selassie, Y.G., Tsegaye, L., 2017. Land Use/Land Cover Factor Values and Accuracy Assessment Using a GIS and Remote Sensing in the Case of the Quashay Watershed in Northwestern Ethiopia. Journal of Natural Resources and Development 38–44. https://doi.org/10.5027/jnrd.v7i0.05.
Tanyaş, H., Kolat, Ç., Süzen, M.L., 2015. A new approach to estimate cover-management factor of RUSLE and validation of RUSLE model in the watershed of Kartalkaya Dam. J. Hydrol. 528, 584–598. https://doi.org/10.1016/j.jhydrol.2015.06.048.
Teng, H.-F., Hu, J., Zhou, Y., Zhou, L.-Q., Shi, Z., 2019. Modelling and mapping soil erosion potential in China. J. Integr. Agric. 18 (2), 251–264. https://doi.org/10.1016/s2095-3119(18)62045-3.
Tsai, F., Lai, J.-S., Nguyen, K.A., Chen, W., 2021. Determining Cover Management Factor with Remote Sensing and Spatial Analysis for Improving Long-Term Soil Loss Estimation in Watersheds. ISPRS Int. J. Geo-Inf. 10 (1) https://doi.org/10.3390/ijgi10010019.
USDA-ARS, User's reference guide: Revised Universal Soil Loss Equation Version 2, Agricultural Research Service https://www.ars.usda.gov/ARSUserFiles/60600505/RUSLE/RUSLE2_User_Ref_Guide.pdf 2008 accessed 12 April 2021.
USDA-ARS, 2013. Science Documentation. Revised Universal Soil Loss Equation Version 2 (RUSLE2): (for the model with release date of May 20, 2008), Agricultural Research Service. https://www.ars.usda.gov/ARSUserFiles/60600505/RUSLE/RUSLE2_Science_Doc.pdf (accessed 12 April 2021).

USDA Sediment sources, yields, and delivery ratios, National Engineering Handbook, Sec. 3: Sedimentation. U.S. Department of Agriculture, Natural Resources Conservation Service 1983 Washington, D.C.
USDA, 2001. Revised Universal Soil Loss Equation Version 2 (RUSLE2), HANDBOOK.
Vami Hermann, N.G.B., Bachir, S.M., Boyossoro, Helene K., Mantuela, D., Fabrice, Y.A., Fernand, K., Eric, Valère D., Kouadio, A., 2018. Cartography and prediction of the risk of water erosion in anyama (district of Abidjan): contribution of RUSLE and markov models. International. J. Hydrol. 2 (6) https://doi.org/10.15406/ijh.2018.02.00137.
Vanmaercke, M., Poesen, J., Broeckx, J., Nyssen, J., 2014. Sediment yield in Africa. Earth-Sci. Rev. 136, 350–368. https://doi.org/10.1016/j.earscirev.2014.06.004.
Vanoni V.A., 1975. Sedimentation Engineering, Manual and Report No. 54. American Society of Civil Engineers, New York.
Vatandaşlar, C., Yavuz, M., 2017. Modeling cover management factor of RUSLE using very high-resolution satellite imagery in a semiarid watershed. Environ. Earth Sci. 76 (2) https://doi.org/10.1007/s12665-017-6388-0.
Vijith, H., Seling, L.W., Dodge-Wan, D., 2017. Effect of cover management factor in quantification of soil loss: case study of Sungai Akah subwatershed, Baram River basin Sarawak. Malaysia. Geocarto Int. 33 (5), 505–521. https://doi.org/10.1080/10106049.2016.1273398.
Villemure, N., 2006. Spatialisation des facteurs de l'érosion en nappe pour une gestion durable des sols en afrique de l'ouest à l'aide des sig et du modèle RUSLE2. Université Du Québec A Montréal.
Vrieling, A., 2006. Satellite remote sensing for water erosion assessment: A review. Catena 65 (1), 2–18. https://doi.org/10.1016/j.catena.2005.10.005.
Vrieling, A., Sterk, G., de Jong, S.M., 2010. Satellite-based estimation of rainfall erosivity for Africa. J. Hydrol. 395 (3–4), 235–241. https://doi.org/10.1016/j.jhydrol.2010.10.035.
Vu, Dinh T., Hoang, N.-D., Tran, X.-L., Turjaman, M., 2021. Evaluation of Different Machine Learning Models for Predicting Soil Erosion in Tropical Sloping Lands of Northeast Vietnam. Applied and Environmental Soil Science 2021, 1–14. https://doi.org/10.1155/2021/6665485.
Wahap, N.A., Shafri, H.Z.M., 2020. Utilization of Google Earth Engine (GEE) for land cover monitoring over Klang Valley, Malaysia. In: IOP Conference Series: Earth and Environmental Science, p. 540.
Walling, D.E., 1983. The sediment delivery problem. J. Hydrol. 65, 209–237.
Wan, S., Li, Q., Cai, T., Li, P., Zou, Zhenhua, 2012. Modeling the Effects of Land-use Change on Sediment Yield in the Upper Huaihe River Basin. China, IEEE International Symposium on Geomatics for Integrated Water Resources Management https://www.doi.org/10.1109/giwrm.2012.6349638.
Wang, B., Zheng, F., Guan, Y., 2016. Improved USLE- K factor prediction: A case study on water erosion areas in China. Int. Soil Water Conserv. Res. 4 (3), 168–176. https://doi.org/10.1016/j.iswcr.2016.08.003.
Wang, B., Zheng, F., Römkens, M.J.M., Darboux, F., 2013. Soil erodibility for water erosion: A perspective and Chinese experiences. Geomorphology 187, 1–10. https://doi.org/10.1016/j.geomorph.2013.01.018.
Wang, G., Wente, S., Gertner, G.Z., Anderson, A., 2002. Improvement in mapping vegetation cover factor for the universal soil loss equation by geostatistical methods with Landsat Thematic Mapper images. Int. J. Remote Sens. 23 (18), 3649–3667. https://doi.org/10.1080/01431160110114538.
Wang, S., Flanagan, D.C., Engel, B.A., 2019. Estimating sediment transport capacity for overland flow. J. Hydrol. 578 https://doi.org/10.1016/j.jhydrol.2019.123985.
Wang, Z., Yang, X., Liu, J., Yuan, Y., 2015. Sediment transport capacity and its response to hydraulic parameters in experimental rill flow on steep slope. J. Soil Water Conserv. 70 (1), 36–44. https://doi.org/10.2489/jswc.70.1.36.
Wangai, P.W., Burkhard, B., Müller, F., 2016. A review of studies on ecosystem services in Africa. International Journal of Sustainable Built Environment 5 (2), 225–245. https://doi.org/10.1016/j.ijsbe.2016.08.005.
Wenner C.G., 1980. Soil conservation in Kenya, especially in small-scale farming in high potential areas using labour intensive methods.
Williams, J.R., 1977. Sediment delivery ratios determined with sediment and runoff models. J. Int. Assoc. Hydrol. Sci. 122, 168–179.
Williams, J.R., Brendt, A.D., 1972. Sediment yield computed with the Universal Equation. Proc. Am. Soc. Civ. Eng. 98 (HY12).
Wischmeier and Smith, 1978. Predicting rainfall erosion losses: a guide to conservation planning. Agriculture Handbook 537. Agricultural Research Service.
World-bank, 2018. Pour que demain ne meure jamais la Côte d'Ivoire face au changement climatique.
Wu, L., Liu, X., Ma, X.-Y., 2017. Research progress on the watershed sediment delivery ratio. Int. J. Environ. Stud. 75 (4), 565–579. https://doi.org/10.1080/00207233.2017.1392771.
Wuepper, D., Borrelli, P., Finger, R., 2019. Countries and the global rate of soil erosion. Nat. Sustainability 3 (1), 51–55. https://doi.org/10.1038/s41893-019-0438-4.
Xiao, J., Moody, A., 2005. A comparison of methods for estimating fractional green vegetation cover within a desert-to-upland transition zone in central New Mexico, USA. Remote Sens. Environ. 98 (2–3), 237–250. https://doi.org/10.1016/j.rse.2005.07.011.
Xin, W., 2020. Temporal and spatial relationships between soil erosion and ecological restoration in semi-arid regions: a case study in northern Shaanxi. China. GiSci Remote Sens. 57 (4), 572–590. https://doi.org/10.1080/15481603.2020.1751406.
Xin, W., Lin, Z., 2020. Soil erosion control practices in the Chinese Loess Plateau: A systematic review. Environ. Dev. 34 https://doi.org/10.1016/j.envdev.2019.100493.
Xu, H., Hu, X., Guan, H., Zhang, B., Wang, M., Chen, S., Chen, M., 2019. A remote sensing based method to detect soil erosion in forests. Remote Sens. 11 (5) https://doi.org/10.3390/rs11050513.
Yang, J., Weisberg, P.J., Bristow, N.A., 2012. Landsat remote sensing approaches for monitoring long-term tree cover dynamics in semi-arid woodlands: Comparison of vegetation indices and spectral mixture analysis. Remote Sens. Environ. 119, 62–71. https://doi.org/10.1016/j.rse.2011.12.004.
Yang, X., 2014. Deriving RUSLE cover factor from time-series fractional vegetation cover for hillslope erosion modelling in New South Wales. Soil Res. 52 (3) https://doi.org/10.1071/sr13297.
Yin, S., Nearing, M.A., Borrelli, P., Xue, X., 2017. Rainfall Erosivity: An Overview of Methodologies and Applications. Vadose Zone J. 16 (12) https://doi.org/10.2136/vzj2017.06.0131.
Zhang, S., Chen, H., Fu, Y., Niu, H., Yang, Y., Zhang, B., 2019. Fractional vegetation cover estimation of different vegetation types in the qaidam basin. Sustainability 11 (3). https://doi.org/10.3390/su11030864.
Zhao, J., Li, J., Liu, Q., Xu, B., Yu, W., Lin, S., Hu, Z., 2020. Estimating fractional vegetation cover from leaf area index and clumping index based on the gap probability theory. Int J Appl Earth Obs. 90 https://doi.org/10.1016/j.jag.2020.102112.
Zhou, J., Fu, B., Gao, G., Lü, Y., Liu, Y., Lü, N., Wang, S., 2016. Effects of precipitation and restoration vegetation on soil erosion in a semi-arid environment in the Loess Plateau, China. Catena 137, 1–11. https://doi.org/10.1016/j.catena.2015.08.015.
Zhu, X., Liu, W., Jiang, X.J., Wang, P., Li, W., 2018. Effects of land-use changes on runoff and sediment yield: Implications for soil conservation and forest management in Xishuangbanna. Southwest China. Land Degrad. Dev. 29 (9), 2962–2974. https://doi.org/10.1002/ldr.3068.
Žížala, D., Juřicová, A., Zádorová, T., Zelenková, K., Minařík, R., 2018. Mapping soil degradation using remote sensing data and ancillary data: South-East Moravia. Czech Republic. Eur. J. Remote Sens 52 (sup1), 108–122. https://doi.org/10.1080/22797254.2018.1482524.